Metamorphism of dry snow as a result of temperature gradient and excess vapor density
by Edward Eagan Adams

A thesis submitted in partial fulfillment of the requirements for the degree of MASTER OF SCIENCE
in Engineering Mechanics
Montana State University

Abstract:
A heat conduction equation to determine the temperature profile in a snowpack is developed. The magnitude of temperature gradient tends to increase as the snow surface is approached, with local minimums through high snow density layers and local maximums above and below these layers. Calculations are made which determine the excess vapor density over the ice grain surfaces which border the pore space. In the presence of a temperature gradient faceted crystals will develop near the top of the pore, as ice is sublimated off of the surfaces in the lower region. Necks will deteriorate most readily, causing an overall weakening of the snowpack. There will be a reduction in the percentage of rounded grains as the faceted form develops. The process is enhanced at warmer temperature and larger temperature gradients. Temperature and excess vapor density are known to determine the habit of ice crystals grown in air. The model predicts excess vapor densities in the snowpack which are similar to those which exist in the atmosphere. Comparison of crystal habits predicted by the model are in good agreement with experimental evidence, when the pore geometry and temperature conditions are specified.

STATEMENT OF PERMISSION TO COPY

In presenting this thesis in partial fulfillment of the requirements for an advanced degree at Montana State University, I agree that the Library shall make it freely available for inspection. I further agree that permission for extensive copying of this thesis for scholarly purposes may be granted by my major professor, or, in his absence, by the Director of Libraries. It is understood that any copying or publication of this thesis for financial gain shall not be allowed without my written permission.

Signature Edward E Adams

Date 6/10/82

METAMORPHISM OF DRY SNOW AS A RESULT OF TEMPERATURE GRADIENT AND EXCESS VAPOR DENSITY

by

EDWARD EAGAN ADAMS

A thesis submitted in partial fulfillment
of the requirements for the degree

of

MASTER OF SCIENCE

in

Engineering Mechanics

Approved:

Chairperson, Graduate Committee

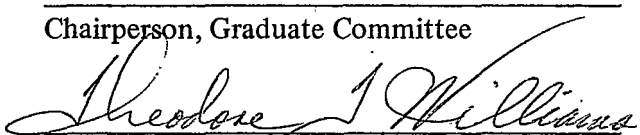

Head, Major Department

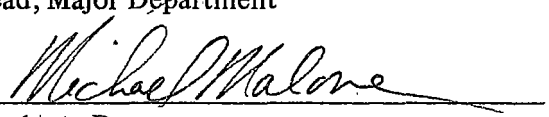

Graduate Dean

MONTANA STATE UNIVERSITY
Bozeman, Montana

May, 1982

ACKNOWLEDGMENTS

I would like to express special thanks to Dr. Robert L. Brown for the guidance and support which he gave, while at the same time encouraging me to pursue the thesis investigation in my own manner.

The work reported here was done under National Science Foundation Grant No. ENG-7901636.

TABLE OF CONTENTS

LIST OF TABLES

LIST OF FIGURES

ABSTRACT

A heat conduction equation to determine the temperature profile in a snowpack is developed. The magnitude of temperature gradient tends to increase as the snow surface is approached, with local minimums through high snow density layers and local maximums above and below these layers. Calculations are made which determine the excess vapor density over the ice grain surfaces which border the pore space. In the presence of a temperature gradient faceted crystals will develop near the top of the pore, as ice is sublimated off of the surfaces in the lower region. Necks will deteriorate most readily, causing an overall weakening of the snowpack. There will be a reduction in the percentage of rounded grains as the faceted form develops. The process is enhanced at warmer temperature and larger temperature gradients. Temperature and excess vapor density are known to determine the habit of ice crystals grown in air. The model predicts excess vapor densities in the snowpack which are similar to those which exist in the atmosphere. Comparison of crystal habits predicted by the model are in good agreement with experimental evidence, when the pore geometry and temperature conditions are specified.

Chapter I

INTRODUCTION

The metamorphism of snow is an ongoing process from the time of its inception in the atmosphere as individual ice crystals, until it eventually returns to the liquid state, as spring runoff or glacial melt water. Ice crystals are formed in the atmosphere when water vapor in clouds is supercooled in the presence of a condensation nuclei, such as dust. A great variety of crystal shapes may result, depending on supersaturation with respect to ice and the temperature under which they form (Nakaya, 1954; Kobayashi, 1961; Mason, Bryant and Van den Heuvel, 1963). All of the crystal types, however, display the same crystal structure. The structure is that of a basal plane with hexagonal symmetry, which is oriented perpendicularly to the principal crystallographic axis.

It is the accumulation of these ice crystals on the ground which forms the basis of a snowpack. Snow is a granular material consisting of ice particles and interstitial pore spaces filled with water, air, and water vapor. It may be classified as dry snow—ice, air, and water vapor, saturated snow—ice and water, and wet snow—where all four constituents are present.

Naturally occurring snowpacks generally exhibit a complex stratigraphy, composed of individual layers of snow which have different properties. These differing snow layers result from the environment to which the snow is subjected when it is on the ground, such as thermal effects, wind, rain or subsequent snowfall, as well as the atmospheric conditions which exist during formation and deposit.

Ice crystals formed in the atmosphere as described above are in a state of unstable thermodynamic equilibrium. In a snowpack, there is a tendency for these intricate crystal

shapes to metamorphose into a more spherical configuration. In the presence of isothermal or near isothermal conditions, this is accompanied by the sintering or bonding together of the ice grains. Sintering leads to an overall strengthening of the snowpack. The entire process is known as destructive or equi-temperature metamorphism. The term equi-temperature may be misleading, since isothermal conditions rarely, if ever, exist naturally in a dry snowpack.

Temperatures at the base of a seasonal snowpack usually remain just below 0° C throughout the winter. Snow is being warmed from below, as the ground gives up heat accumulated during the warmer months. If this geothermal heating condition coincides with cooler ambient air temperatures, characteristic of the winter months, a temperature gradient is established across the snowpack. A similar situation will also exist on temperate glaciers or polar ice which has been warmed during the summer. Temperature gradients, measured from the ground toward the snow surface, between -1.0 to -10.0 deg m^{-1} are reported to be typical in alpine snowpacks (Yosida, 1963), while gradients of -30.0 deg m^{-1} occur annually on the Greenland ice sheet (Benson, 1962). Trabaut and Benson (1972) report normal gradients of -100.0 deg m^{-1} and as high as -200.0 deg m^{-1} in central Alaska.

A variation in vapor pressure, resulting from the temperature differential, will cause a mass flux of vapor from the zone of high pressure, the deeper warmer region, to the zone of lower vapor pressure. Since dry snow, in which this mechanism is most effective, consists of a solid and a vapor phase of the same material, the migration of mass need not take place exclusively through the tortuous labyrinth of pore spaces. The transfer can take place through the solid matrix itself, as a "hand to hand" transfer of mass (Yosida and

Kojima, 1950, from Akitaya, 1974). Vapor will evaporate from the top of an ice grain diffuse across the pore and deposit as a solid on the bottom of the grain above. The ice molecules on the top of this grain will likewise sublimate and redeposit in a similar fashion.

When snow of low to medium density is subjected to the correct combination of temperature and temperature gradient, angular flat surfaced crystals, known as depth hoar, will develop at the expense of those grains with a more rounded configuration. This effect is most prevalent in low density snow at relatively warm temperatures subjected to large temperature gradients. Consequently, depth hoar crystals develop most readily early in the snow season, when the pack is shallow and therefore large temperature gradients exist, in association with a relatively warm average snow temperature.

Two general types of depth hoar are recognized (Akitaya, 1974); a solid type, which develops under smaller temperature gradients, and a skeleton type which predominates under large temperature gradients. Skeleton type depth hoar is composed of large faceted crystals, which are poorly bonded together and form a weak snow layer. The solid type consists of small faceted crystals which do not show the marked reduction in strength characterized by the skeleton type.

Snowpack development in which faceted crystal growth predominates is known as constructive or temperature gradient metamorphism. Crystal development will take place in three stages. Early crystal development is known as anhedral, partially developed crystals are called subhedral, and the advanced form are termed euhedral crystals. Snow which has undergone this temperature gradient process is characterized by an overall reduction in strength, particularly during the intermediate subhedral crystal development (Bradley, Brown, and Williams, 1977; Adams and Brown, 1982). Weak zones in the pack resulting

from temperature gradient metamorphism are a major cause of snow avalanches. An understanding of the process is therefore of practical concern.

Akitaya (1974), in what is perhaps the most complete experimental work carried out on the topic of temperature gradient metamorphism, has shown that pore size, initial ice grain size and geometry effects depth hoar development. A large pore will enhance the rate of growth and the size of the crystal which will develop. This is in agreement with Marbouty's (1980) observation that fine grained snow with a density in excess of approximately 350 $KG\text{-}M^{-3}$ subjected to even a large temperature gradient will develop solid type depth hoar. Lower density snow, which has a larger pore space tends toward the skeleton type in the presence of a sufficient temperature gradient.

Faceted crystals which develop in the snow have a preferential direction of growth (Akitaya, 1974). Crystals grow toward the direction of higher temperature. This was demonstrated by imposing positive and negative temperature gradients on the snow samples. The direction of crystal growth was shown to be dependent on the thermal gradient and not on gravity.

Several types of crystals will develop simultaneously in a particular layer with one form being predominant. The predominant crystal type was observed to be a function of temperature and temperature gradient (Figure 1) (Akitaya, 1974; Marbouty, 1980). Earlier studies by Nakaya (1954), Hallet and Mason (1958), Kobayashi (1961), Mason, Bryant, and Van den Heuvel (1963) and others have investigated the growth of ice crystals in air. Their results show the correlation between crystal habit, temperature and excess vapor density (or supersaturation) in air relative to the equilibrium vapor pressure over ice. Results observed by Kobayashi are displayed in Figure 2.

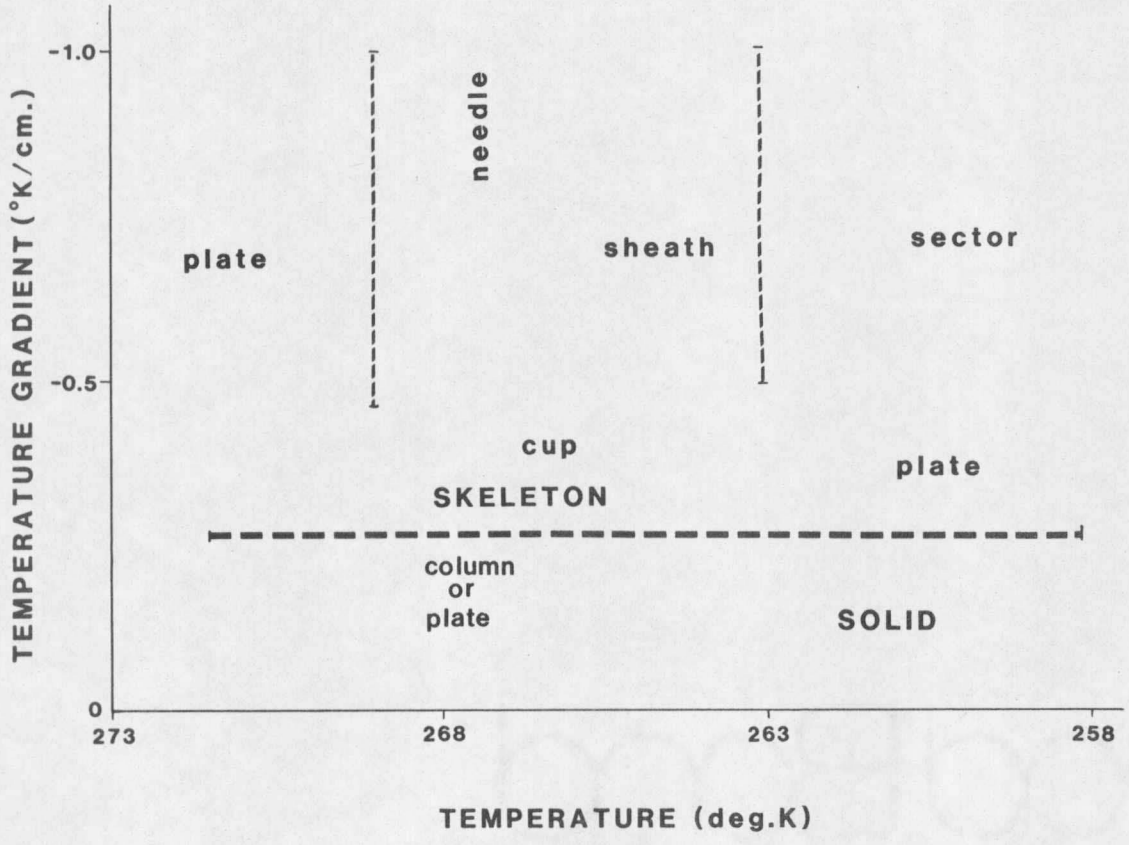

Figure 1. Dependence of Crystal Habit Development in a Snowpack on Temperature and Temperature Gradient (Akitaya, 1974).

It seems as if there must be some correlation between crystals grown from vapor in the air and those which grow in snow subjected to a temperature gradient. This becomes apparent when the observances of Kobayashi (1961) (Figure 2) for crystals grown in air are compared to those of Akitaya (1974) (Figure 1), for the same temperature range.

Examining these diagrams it becomes evident that the temperature gradient in the snow must in some way affect the excess vapor density. It is the temperature of formation which governs the crystal habit and the excess vapor density (or supersaturation) which determines the secondary growth features (Mason, Bryant, and Van den Heuvel, 1963). The basic crystal habit may take the form of either a plate or a prism. Whether a crystal is considered a plate or a column is determined by the ratio of the principal (c) axis to the basal (a) axis. For a plate structure c/a is less than 1, whereas if c/a is greater than 1, the crystal is considered a prism. Secondary growth features alter the appearance of the crystal habit such as dendritic extensions on plate crystals or prisms taking on a cup shaped appearance.

It is the purpose of this paper to further the understanding of depth hoar development. An analytic development is presented which represents an attempt to describe the thermodynamic processes involved in temperature gradient metamorphism.

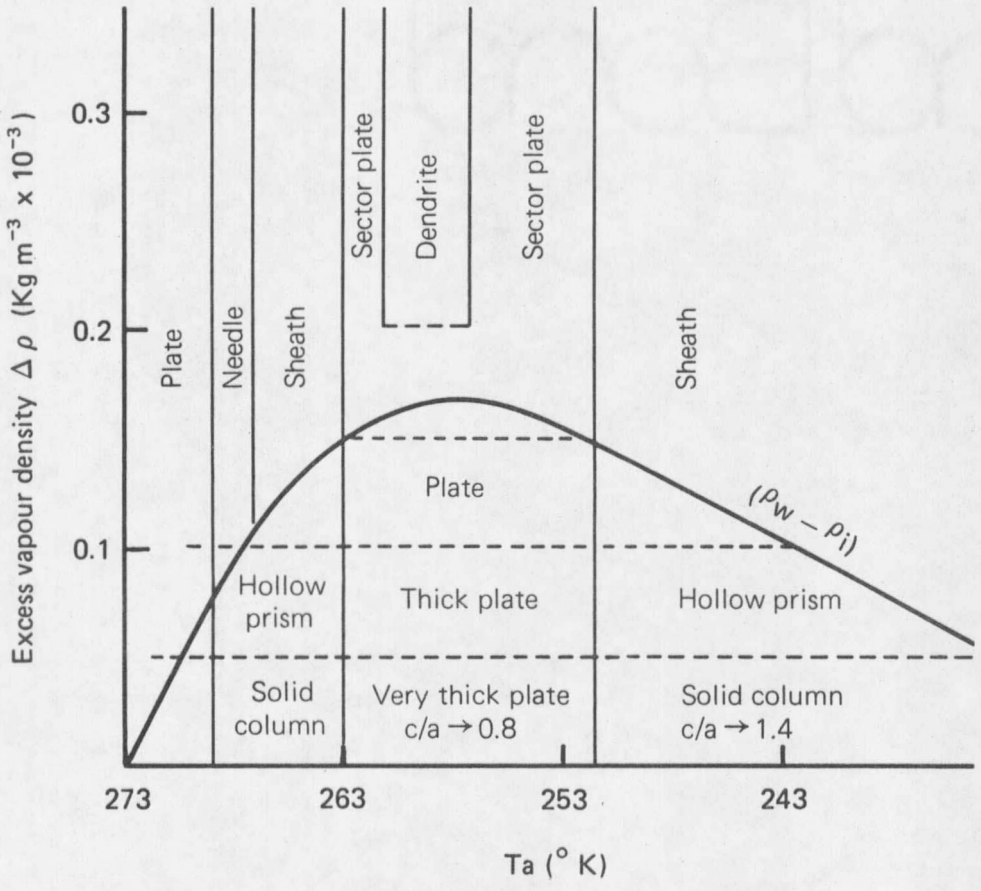

Figure 2. Crystal Habit of Ice Grown in the Atmosphere Based on Temperature and Excess Vapor Density (Kobayashi, 1961).

Chapter II

HEAT FLOW IN A SNOWPACK

When all mechanical effects are neglected the general isotropic form of the Fourier heat conduction equation may be written as

$$\frac{\partial}{\partial x}\left(k\,\frac{\partial T}{\partial x}\right) + \frac{\partial}{\partial y}\left(k\,\frac{\partial T}{\partial y}\right) + \frac{\partial}{\partial z}\left(k\,\frac{\partial T}{\partial z}\right) + Q = \rho_s C\,\frac{\partial T}{\partial t} \qquad (1)$$

Where k is the thermal conductivity, T is temperature, Q is the internal heat generation per unit time per unit volume, $\rho_s C\,\partial T/\partial t$ is the rate of internal energy change per unit volume, t is time, ρ_s is the snow density, C is the specific heat of ice (Bozey and Wienke, 1960).

In the presence of a temperature gradient such as that discussed in the Introduction, heat flow in a natural snowpack occurs in the direction normal to the slope of the ground. This is taken to be the z coordinate direction. There will be no flow of heat in the x and y component directions, which are taken as tangent to the slope, since the snow cover may be considered as extending infinitely in this plane.

Using the ground snow interface as the origin for the z axis, a negative temperature gradient $\partial T/\partial z$ is established in the snowpack, since the ground is in general warmer than the upper regions of the snow. The flow of heat will be from the warmer ground toward the cooler snow surface. Positive gradients may occur near the snow surface due to diurnal fluctuations or periods of warmer weather. A positive gradient throughout the pack will not generally persist naturally, since this indicates a prolonged surface temperature above 0° C, in order to be significantly warmer than the ground. This will cause melting in the upper part of the pack. Meltwater then percolates downward through the snow, finally

achieving a constant temperature near 0°C throughout. This type of wet or saturated isothermal snowpack is characteristic of late spring snow conditions in alpine regions.

Internal heating within the snowpack will be generated during metamorphism as mass is sublimated off of, and deposited onto the ice surfaces. The net quantity of heat produced or lost may be calculated from the energy released due to the latent heat of sublimation, as the mass of water undergoes this phase transformation. Internal heat generation for Equation 1 may be expressed as

$$Q = - L \frac{\partial J_s}{\partial z} \tag{2}$$

Where L is the latent heat of sublimation and J_s is the mass flux of the snow.

Equation 1 may now be written for snow as

$$\frac{\partial}{\partial z} (k \frac{\partial T}{\partial z}) - L \frac{\partial J_s}{\partial z} = \rho_s C \frac{\partial T}{\partial t} \tag{3}$$

Once again neglecting mechanical effects, a change in the snow density is the result of water vapor being driven upward through the snow. The conservation of mass in the snow may then be expressed by

$$\frac{\partial J_s}{\partial z} = - \dot{\rho}_s \tag{4}$$

$\dot{\rho}_s$ is the time rate of change of snow density.

Thermal conductivity of snow is a function of a number of parameters such as density, temperature, intergranular bonding and to a lesser degree on grain size and grain shape, as well as any other parameters which would facilitate or impede the transfer of heat. The thermal conductivity of ice is much greater than that of water vapor at the same temperature. Consequently the major portion of heat transfer by pure conduction will take

place through the solid ice network, rather than the pore. This is the reason thermal conductivity is strongly dependent on snow density. However, part of the heat is carried upward by diffusion through the pore space as well. Because of this, an effective thermal conductivity coefficient instead of the true conductivity is used to determine the snowpack temperature profile.

Palm and Tveiteroid (1979) have concluded theoretically, that in deep layers of highly permeable snow subjected to very large temperature gradients, thermal convection may be an effective means of vapor flux and therefore heat flux. In conditions occurring naturally in central Alaska, U.S.A., it has been shown that convection can indeed be significant to the flow of mass and heat. The significance of convection in this region is the result of the extreme conditions prevalent there. A shallow snowpack 0.5 to 0.8 m thick is subjected to approximately 200 consecutive days of excessive thermal gradients. Gradients of -200 deg m^{-1} have been observed and -100 deg m^{-1} are considered common.

Investigation by Akitaya (1974), on natural snow samples, indicate that convection did not occur even when gradients of -200 deg m^{-1} were artificially induced, although the duration of the experiment was much shorter than those observed in central Alaska. He was able to achieve convection only when an extremely permeable artificial snow was constructed. Individual ice grains for the sample were represented by cubes of fine grained compacted snow 0.15 m on a side. Using this "snow," temperature gradients greater than 100 deg m^{-1} were necessary before convection was assumed to occur.

The model presented in the paper will ignore the effects of thermal convection. Porosity, temperature gradient magnitude and the duration necessary to initiate significant

thermal convection are much larger than those encountered in most alpine regions of the world or even on the Greenland ice sheet.

Empirical expressions which are generally used to determine the thermal conductivity coefficient are based solely on snow density. For a partial list of examples, see Mellor (1964). Since density is certainly not the sole parameter by which conductivity should be measured, the data accumulated by Voitkovsky, Golubey, Lapteva, Troshkina, Ushakova, and Pavlov (1976) has been utilized. Voitkovsky et al. obtained what they considered to be values near the true conductivity as a function of density. These values were obtained by taking measurements at very low temperatures, where diffusion is not as effective a means of heat transfer. Statistical methods were used to arrive at a true thermal conductivity coefficient.

$$k_t = 0.030 + 0.303\,\rho_s - 0.177\,\rho_s^2 + 2.250\,\rho_s^3 \qquad (5)$$

where the snow density ρ_s is in c.g.s. units.

Data collected in the same region (Yakutsk, USSR) for conduction as a function of temperature is represented in Figure 3, by the solid line. The relationship of the conductivity as a function of temperatures is approximately exponential. The measurements were taken for snow at a density of 0.25 gm cm^{-3}.

Using the data collected in Yakutsk, an expression to determine the effective thermal conductivity coefficient as a function of two parameters, density and temperature, is

$$k = \gamma \exp[\beta T]\, k_t \qquad (6)$$

The constants γ and β were determined by evaluating Equation (6) for ρ_s equal to 0.25 gm cm^{-3} and temperatures of 253°K and 268°K. Values for conductivity, as a function of temperature, are based on the data collected in Yakutsk shown in Figure 3. Values

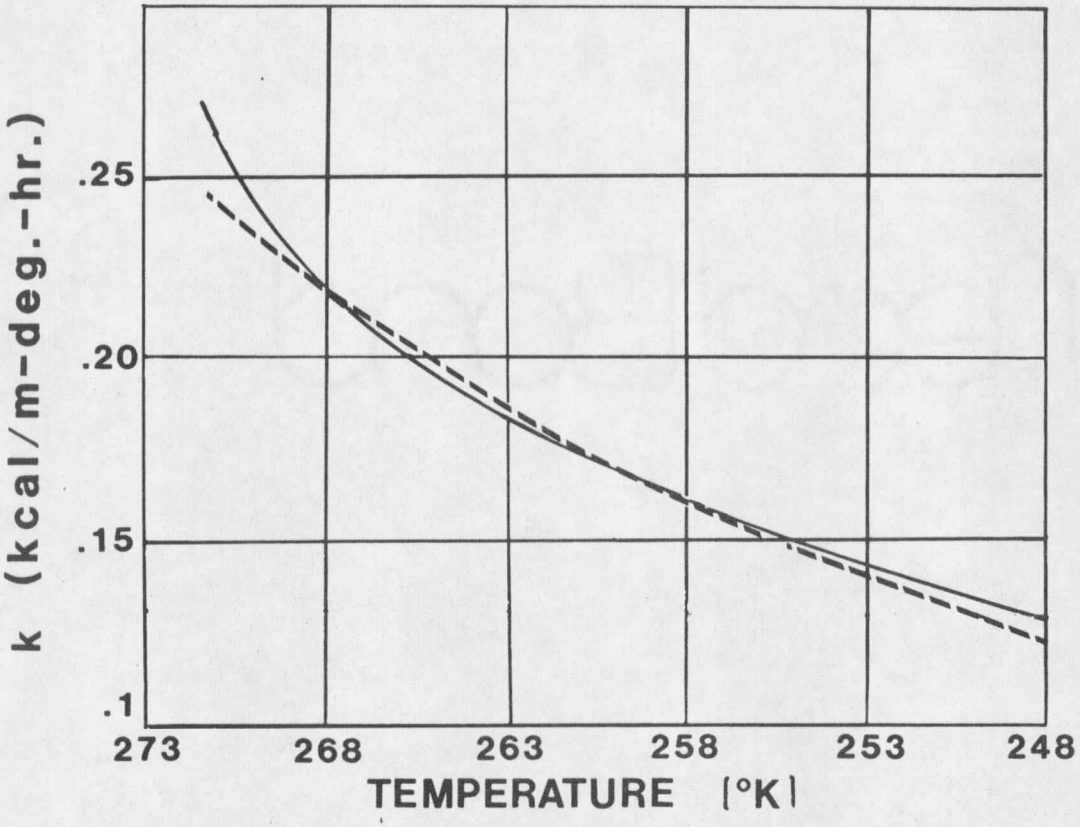

Figure 3. The Solid Line Represents the Thermal Conductivity as a Function of Temperature (Voitkovsky, 1976). The Dashed Line Represents the Derived Effective Thermal Conductivity.

for γ of 9.404×10^{-4} and β of 0.028 result. The dashed line in Figure 3 shows the conductivity calculated using Equation 6 with the determined constants. To maintain units which are consistent with the rest of this paper. Equation (6) is multiplied by 1.162. Units of thermal conductivity are J m^{-1} deg^{-1} sec^{-1}. Finally the equation in m.k.s. units which is used to evaluate the effective thermal conductivity coefficient of snow is

$$k = (1.093 \times 10^{-3}) \exp(0.028T)[0.030 + 0.303(\rho_s \times 10^{-3}) - 0.177(\rho_s \times 10^{-3})^2 + 2.250(\rho_s \times 10^{-3})^3] \quad (7)$$

Although this cannot be considered a truly accurate measure of effective thermal conductivity, the expression does represent an attempt to utilize two important parameters which are easily measurable.

No data is available which indicates the dependence of thermal conduction on intergranular bonding. This is unfortunate since the manner in which the bonds, or necks, join the ice grains must be significant to the thermal conduction in the snow. Well bonded snow with large necks will facilitate heat flow more readily than poorly sintered snow of the same density, since the conductivity of ice is higher than that of water vapor.

Substituting $-\dot{\rho}_s$ from Equation (4) for $\partial J_s/\partial z$ in Equation (3) and recognizing that the thermal conductivity coefficient for snow will vary with position in the snowpack, a Fourier heat conduction equation for snow is

$$k \frac{\partial^2 T}{\partial z^2} + \frac{\partial k}{\partial z} \frac{\partial T}{\partial z} + L\dot{\rho}_s = \rho_s C \frac{\partial T}{\partial t} \quad (8)$$

Chapter III

CALCULATING THE TEMPERATURE PROFILE

To calculate the temperature distribution vertically throughout the snowpack, Equation (8) must be solved. In order to easily determine the temperature profile for numerous snowpacks with varying stratigraphy, the heat conduction equation must be solved by an approximate solution method, in this case the finite difference method.

The finite difference form for Equation (8) is

$$\frac{k_i^n}{\Delta z^2}(T_{j+1}^n - 2T_j^n + T_{j-1}^n) + \frac{(k_{j+1}^n - k_{j-1}^n)}{2\Delta z}\frac{(T_{i+1}^n - T_{j-1}^n)}{2\Delta z} + L\frac{(\rho_{sj}^{n+1} - \rho_{sj}^n)}{\Delta t}$$

$$= \frac{\rho_{sj}^n (T_j^{n+1} - T_j^n)}{\Delta t} \qquad (9)$$

where the subscript i indicates the values for position z which are to be evaluated, and the subscript n indicates the values for time t.

Akitaya (1974) in field observations taken over an entire winter season noticed a general increase in the density of snow which was consistently influenced by a thermal gradient. This rise in density can be attributed to mechanical settlement and compaction due to gravity, and perhaps to some degree on mass flux into these layers. Similar results have been observed by Giddings and La Chapelle (1962). Measurement of density change in the presence of thermal convection (Trabant and Benson, 1972) show little change after the initial compaction of new snow. This indicates that the increase in density due to settlement is counterbalanced by the mass lost due to vapor flux resulting from the thermal convection.

Four years of data were collected in the high altitude continental climate of Colorado, USA (Armstrong, 1980), on the relation between compressive strain rates, thermal

metamorphism, and density, for dry snow. Armstrong concluded that large differences in density which exist between equi-temperature and temperature gradient metamorphosed snow is the result of differential strain rates, rather than significant mass flux due to diffusion.

Marbouty (1980) has conducted a series of precisely controlled laboratory experiments. He found that after the initial settlement and compaction which accompanies destructive metamorphism of new snow, there was no change in the density of snow subjected to negative temperature gradients as large as 66.0 deg m^{-1}. In the controlled environment of a laboratory setting, where no wind or additional snow is added which would mechanically compact the snow, the depth of the samples remained constant and no settlement or densification occurred.

Although there is probably some change in snow density as the result of diffusion alone, it is difficult to measure and is presently considered to be slight. When mechanical effects such as compaction and settlement, and the thermal effects of vapor flow due to convection are ignored, the rate of change of density term in Equations (8) and (9) can be ignored.

The equation which was used to solve for the temperature distribution is arrived at by eliminating the time rate of change of density $\dot{\rho}_s$ term and algebraically manipulating Equation (9). This yields

$$T_j^{n+1} = \frac{k_j^n \Delta t}{\rho_{sj}^n C \Delta z^2}(T_{j+1}^n + T_{j-1}^n) + \frac{\Delta t(k_{j+1}^n - k_{j-1}^n)(T_{i+1}^n - T_{j-1}^n)}{4\,\rho_{sj}^n C \Delta z^2}$$

$$+ \left(1 - \frac{2\,k_j^n \Delta t}{\rho_{sj}^n C \Delta z^2}\right) T_j^n \qquad (10)$$

A final temperature profile is calculated by assuming constant boundary conditions at the bottom and top nodes, which represent the ground-snow interface and snow surface, respectively. Temperatures used are those which are deemed appropriate boundary conditions for a snowpack. Isothermal initial conditions at the same temperature as the surface node are assumed throughout the snowpack. Equation (10) is then incremented on time until a steady state heat flow is achieved. A final temperature gradient distribution is calculated by numerically differentiating this steady state solution.

$$TG_j^n = \frac{(T_{j+1}^n - T_{j-1}^n)}{2\Delta z} \tag{11}$$

where TG is the temperature gradient.

Oscillating boundary conditions, typical of a natural environment could be used in the model to simulate diurnal or climatic temperature fluctuations. More realistic initial conditions could also be used if such information is available. However, given sufficient time more accurate initial conditions would have little effect, since the final temperature profile is governed by the boundary conditions and snow density.

Chapter IV

VAPOR PRESSURE IN THE PORE

Since depth hoar crystals are grown from the vapor phase, development of these crystals must be restricted to the pore spaces in a snowpack. For this reason, an analysis of vapor pressure within the pore is carried out. Excess vapor densities (or supersaturation) at several regions of a pore with a temperature gradient imposed on it are examined, in an effort to understand the relationship between depth hoar crystal development, the associated reduction in the percent of rounded ice grains, the preferential direction of faceted crystal growth, and the reduced strength of a layer in which temperature gradient metamorphism occurs. A schematic representation of the pore for this one dimension flow analysis is shown in Figure 4.

The mass flux of water vapor across a pore in the presence of a temperature gradient can be described by

$$J = - \frac{D}{RT} \frac{dP_v}{dz} \tag{12}$$

where J is the mass flux of water vapor across the pore, D is the diffusion coefficient, R is the gas constant for water vapor, T is temperature, P_v is the vapor pressure in the pore, and z is the coordinate in which direction the temperature gradient acts.

From continuity we have

$$\frac{dJ}{dz} = - \dot{\rho}_v \tag{13}$$

where $\dot{\rho}_v$ is the time rate of change of vapor density. Vapor density is taken to be constant at any particular temperature and at every depth. The time rate of change of density therefore is zero,

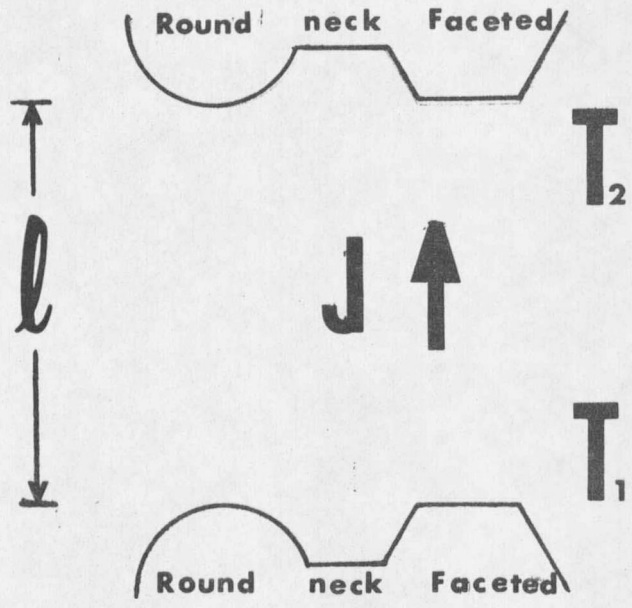

Figure 4. A Schematic Representation of the Idealized Pore Which is Used in the Model. The Round Grains are Represented by Spheres and the Necks by Cylinders. ℓ is the Pore Height and Taken to be the Same for all Three Shapes, J is Mass Flux and T is Temperature. The Direction of J Shown is Valid for $T_1 > T_2$.

$$\dot{\rho}_v = 0 \tag{14}$$

The diffusion coefficient, D, is dependent on temperature (Giddings and La Chapelle, 1962) as

$$D = \alpha T^{1.7} \tag{15}$$

where α is a proportionality constant.

Equations 12, 13, 14, and 15 can be combined to give

$$\frac{d}{dz}\left[\frac{\alpha T^{.7}}{R}\frac{dP_v}{dz}\right] = 0 \tag{16}$$

$$\frac{\alpha T^{.7}}{R}\frac{dP_v}{dz} = A \tag{17}$$

where A is a constant of integration.

$$\frac{dP_v}{dz} = \frac{AR}{\alpha T^{.7}} \tag{18}$$

Integration gives

$$P_v = \frac{AR}{\alpha}\int_o^z \frac{dz}{T^{.7}} + P_v(z=o) \tag{19}$$

$$= \frac{AR}{\alpha}\int_o^z \frac{dT}{T^{.7}}\frac{dz}{dT} + P_{vo} \tag{20}$$

$$= \frac{AR}{\alpha}\frac{1}{(\frac{dT}{dz})}\int_{T_o}^{T_z}\frac{dT}{T^{.7}} + P_{vo} \tag{21}$$

$$= \frac{AR}{\alpha}\frac{1}{(\frac{dT}{dz})}\frac{T^{.3}}{0.3}\Bigg|_{T_o}^{T_z} + P_{vo} \tag{22}$$

A constant temperature gradient across the pore was assumed in the above. Water vapor pressure as a function of temperature and position in the pore is therefore

$$P_v = \frac{AR}{\alpha} \frac{3.333}{(\frac{dT}{dz})} (T^{-3} - T_o^{-3}) + P_{vo} \quad (23)$$

Each pore boundary is composed of a variety of crystal surface shapes. Three basic shapes are of concern here, grains with a predominately rounded configuration, faceted crystals composed of flat surfaces and necks which join the grains together and determine the overall snow strength.

The mean radius of curvature, r, for these crystal shapes is determined by

$$\frac{2}{r} = \frac{1}{r_1} + \frac{1}{r_2} \quad (24)$$

where r_1 and r_2 are the two principal radii of curvature, or the radii of curvature measured in any two orthogonal planes.

Colbeck (1980) states the equilibrium vapor pressure, P, over an ice grain surface varies with temperature and mean radius of curvature. A relationship between saturation vapor pressure and temperature may be found by utilizing the Clausius-Clapeyron equation for a particular radius of curvature.

$$\frac{dP}{dT} = \frac{PL}{RT^2} \quad (25)$$

$$\int_{P_o}^{P} \frac{1}{P} dP = \int_{T_o}^{T} \frac{L}{RT^2} dT \quad (26)$$

where P_o is a reference pressure and T_o is the corresponding reference temperature.

$$\text{Ln} [\frac{P}{P_o}] = \frac{L}{R} (\frac{1}{T_o} - \frac{1}{T}) \quad (27)$$

and the vapor pressure as a function of temperature becomes

$$P(T) = P_o \exp[\frac{L}{R}(\frac{1}{T_o} - \frac{1}{T})] \tag{28}$$

The vapor pressure in terms of the mean radius of curvature at a fixed temperature may be examined by Kelvin's equation.

$$P(r) = P_o \exp[\frac{1}{\rho_i R T_o} \frac{2\sigma}{r}] \tag{29}$$

P_o and T_o are the reference pressure and temperature. These are taken to be the same values as those used in Equation (22), ρ_i is the density of ice, and σ is the interfacial energy.

A single expression for the saturation vapor pressure over the grain surfaces can be found by combining the Clausius-Clapeyron (24) and the Kelvin (25) equations. The saturation vapor pressure in terms of the temperature and mean radius of curvature is

$$P(T,r) = P_o \exp[\frac{2\sigma}{\rho_i R T_o r}] \exp[\frac{L}{R}(\frac{1}{T_o} - \frac{1}{T})] \tag{30}$$

Under the influence of a constant temperature gradient, the temperature is assumed to vary linearly across the pore,

$$T(z) = \frac{dT}{dz} z + T(o) \tag{31}$$

where T(o) is the temperature at the bottom of the pore.

Vapor pressure over the ice surfaces which comprise the upper and lower boundaries of the pore are determined from Equation (30). These results give the boundary conditions which are used to solve for the constants A and P_{vo} in Equation (23), for each radius of curvature. The vapor pressure at the upper and lower boundaries of the pore is determined by the temperature and the relative densities of grains with rounded geometry, faceted geometry and of the necks. These all contribute to the vapor pressure at the pore bounda-

ries. The total vapor pressure must therefore be the sum of the contributions of ice grains with particular radii of curvature and of the necks. The vapor pressure in the pore can now be calculated by evaluating Equation (23) at the center of the pore for each radius of curvature, and dependent on the density of crystals with that particular radius of curvature. Explicitly the pore pressure is taken to be

$$P_v = \sum_{m=1}^{n} \frac{A_m R}{\alpha} \frac{3.333}{\left(\frac{dT}{dz}\right)} \left[T\left(\frac{\ell}{2}\right)^{.3} - T_o^{.3}\right] + P_{o(m)} \frac{\rho_m}{\rho_s} \qquad (32)$$

where the subscript m indicates a particular radius of curvature, n is the total number of different radii, ρ_m is the density of crystals with r_m radius, ρ_s is the density of snow, and ℓ is the height of the pore. In this way, the effect of the different grain radii are weighted by their relative densities at the pore boundaries.

It should be noted here that the solution given by Equation (23) gives a nonlinear variation in the vapor pressure as z is varied from 0 at the bottom of the pore to ℓ at the top of the pore. This effect shows up in the final calculation of vapor pressure by Equation (32). Physically the temperature gradient induces a slight bulge in the pore vapor pressure near the center of the pore.

In order to examine the vapor densities associated with various crystal shapes, a simplified pore geometry is assumed. The rounded grains are modeled as spheres and a single radius size is assumed. Streological methods have shown that necks are best modeled as a cylinder (Kry, 1975). Here also a single radius size is assumed for ease of calculation and analysis. The flat crystals display an infinite radius of curvature.

Mean pore size is determined by snow density and the size of the ice grains. A linear regression routine was utilized to achieve an expression by which the pore size could be determined. The equation which was arrived at, based on a limited number of thin sections of predominately round grains taken by Akitaya (1974), is

$$\ell = 0.003553 - 0.7772 \times 10^{-5} \rho_s + 2.312 r_r \tag{34}$$

where r_r is the mean radius of curvature of the round grains.

Although perhaps only marginally valid statistically, the results calculated were reasonable for pore size as a function of the snow densities and grain sizes used.

Utilizing the described formulation, excess vapor densities at the pore boundaries have been computed for a variety of snow densities, crystal sizes and temperature conditions. The excess vapor pressure is defined here as the difference between the pore vapor density and the vapor density associated with the grain surface. Under the influence of a temperature gradient, the excess vapor density is greatest at the upper pore boundary. This causes the crystal growth rate to proceed most rapidly in this region. The predominant crystal habit, therefore, is determined by the temperature and excess vapor density in the upper region of the pore.

Chapter V

RESULTS AND CONCLUSIONS

All of the values calculated for use in this paper are based on idealized snow. For the sake of simplicity, clarity and consistency in comparison a single snow depth of 0.95 m, in which 95 percent of the snow density is composed of rounded grains, 4 percent faceted and 1 percent necks, is used for all of the samples. In examining the graphs related to the theoretical snowpacks displayed throughout this section, care should be taken to notice the scale of the ordinate axis. The scale is varied from case to case, based on maximum and minimum values of the dependent variable. This was done to accentuate contrast in the data which is plotted.

Results which Equation 10 yields for temperature are first examined by considering homogeneous snow. In doing so, the effect which temperature has on the thermal conductivity and, hence, on the temperature profile, may be examined. Snow with a density of 200 $KG \cdot m^{-3}$ is subjected to several different surface temperature boundary conditions. When the temperatures at the base and the surface are relatively close, as in Figure 5, with a five degree differential, a nearly linear temperature distribution with depth is produced. As the difference in temperature is increased, the deviation from a linear temperature profile increases (Figures 6, 7, 8).

A change in density will also have an effect on the temperature profile. However, different densities of homogeneous snow samples subjected to the same temperature boundary conditions will give similar temperature distributions. This is graphically demonstrated by comparing Figure 8, which is the temperature profile for snow with a density of 200 $KG \cdot m^{-3}$, and Figure 9, which is for a snow density of 100 $KG \cdot m^{-3}$.

Large differential temperature boundary conditions of 273°K and 233°K are chosen for snow samples 2 through 7. Density layering, the temperature profile, temperature gradient distribution, and the maximum excess vapor density distribution are shown graphically for each sample stratigraphy in Figures 8 through 28. In addition, Tables 1 through 6 give the detailed results of the analysis of conditions in a pore at each node for snow samples 2 through 7.

Figure 9 reveals the temperature profile for a homogeneous 100 $KG \cdot m^{-3}$ density snow. Figure 10 is the corresponding temperature gradient distribution. Results displayed in Figure 10 indicate that the magnitude of the temperature gradient becomes larger as the snow surface is approached from the bottom. This is in agreement with Akitaya's (1974) observations in a natural snowpack, "A snow layer near the surface is subjected to a consistent large negative temperature gradient when air temperature is maintained for a long period. . . . Near the bottom of a snow cover, a very small negative temperature gradient is maintained through a winter season after the snow cover gets a sufficient thickness."

Excess vapor density as stated previously is taken to be the difference between the vapor density in the pore and that over the ice surface. The excess vapor density term is arrived at by dividing the pressure difference from Equations 32 and 30 by the gas constant for water vapor and the temperature at the ice surface.

The maximum excess vapor density within the pore will determine the predominant type of crystal which will form, because growth will proceed most readily here. This maximum excess vapor density will be at the top of the pore over the flat ice surfaces. Crystal development which occurs at low supersaturations will have the form of columns or plates, depending on temperature (Figure 2). Therefore, new growth in the pore will be in the

form of faceted crystals, near the top of the pore. Maximum excess vapor density profiles which are shown graphically are calculated in this region. If only rounded surfaces and necks are present initially, faceted crystal growth will develop on the rounded surfaces, and flat surfaces will be produced.

An analysis of Figure 11 shows that the maximum excess vapor density decreases at lower temperatures, even in the presence of an increasing magnitude of temperature gradient (Figure 9). This demonstrates analytically why depth hoar is observed to grow more readily in the lower regions of the snowpack than it does in the upper regions, even when the negative temperature gradient is greater in magnitude at the higher elevation.

Further insight into the temperature gradient metamorphic process is obtained by referring to Tables 1 through 6. Excess vapor densities over the rounded surfaces, the flat surfaces and the necks at the top and bottom of the pores are examined. There is an overall positive excess vapor density over the ice surfaces in the upper region of the pore and a negative excess vapor density over the surfaces on the bottom. This causes a migration of mass from the lower to the upper regions of the pore. The process, as described, is in agreement with the "hand to hand" transfer of mass described by Yosida and Kojima (from Akitaya, 1974). The excess vapor density imbalance also accounts for the preferential direction of growth of depth hoar crystals as observed by Akitaya (1974).

Undersaturation (negative excess vapor density) over the ice surfaces in the lower region of the pore is greatest over the necks, second over the rounded and least over the flat surfaces. Undersaturation causes the sublimation of mass off of the ice surfaces involved. Therefore, mass is most readily sublimated from the necks. This leads to a reduc-

tion in size of the bonds which join the ice grains together, and an ensuing weakening of the snow layer.

Rounded ice grains near the bottom of the pore will sublimate more readily than the flat surfaces at the same level. New development in the pore, as previously stated, will form either plates or columns. As a result, there is a decline in the density of rounded grains, while the density of the faceted form increases. As the radius of the rounded grains and necks decrease, there is a rise in the vapor pressure over these surfaces (Equation 30), accompanied by a larger undersaturation over the surfaces near the bottom of the pore. Growth of the faceted form will provide additional area for accumulation. These developments together should further facilitate the metamorphic process.

Homogeneous snowpacks rarely exist in nature. Layers of dense snow resulting from wind, sun, rain, atmospheric conditions of deposition, etc., are usually present to form a more complex stratigraphy. Effects of this density layering on metamorphism is examined next. Sharp contrasts in density are used so that pronounced effects of layering may be examined.

Consider first, a snowpack of 100 $KG \cdot m^{-3}$ density with a surface crust of 400 $KG \cdot m^{-3}$ density (Figure 12). The temperature profile throughout the pack is altered from that of the homogeneous pack, as a result of the crust. Compare Figures 9 and 13. The crust produces an increase in temperature gradient beneath the crust and a reduction in the gradient through the crust (Figure 14). Excess vapor density is substantially increased near the base (Figures 11 and 15), demonstrating that layering in upper regions of the snow may significantly affect metamorphism in the lower more thermodynamically active regions.

It may be noted at this point, that an increase in magnitude of the temperature gradient will cause a greater excess vapor density in the upper region of the pore and a more negative excess vapor density in the lower region, if all other parameters remain the same. This situation may be examined by referring to depth 0.00 in Tables 1 and 2. Development of faceted crystals, reduction of snow strength and a decrease in the density of rounded grains is enhanced when the magnitude of the temperature gradient is increased.

When the high density layer is placed toward the center of the 0.95 m sample 4 (Figure 16), a larger excess vapor density than that of the the previous example is produced in the lower region of the snow (Figure 19). The excess vapor density through the dense layer is very low, indicating that faceted crystal growth is less prevalent here. This is true, because of the smaller pore size associated with higher density snow, as well as the smaller temperature gradient produced by the higher thermal conductivity. Although the excess vapor density increases above the layer, it remains lower than at the same level in the homogeneous sample (Figure 11).

A layer placed near the bottom (Figure 20) will cause a rise in the maximum excess vapor density, compared to the homogeneous snow, on both sides of the crust. In this case the layer produces a major increase in the excess vapor density above the crust (Figure 23). Faceted crystal growth associated with the zones of the high excess vapor density shows excellent correlation with observations in a natural environment. Development of depth hoar crystals in the field are known to occur both immediately above and below crusts, but growth above the layers is more common and is most frequently seen when the temperature is near 273°K (Perla, 1978).

The effect of several layers of high density snow in a close proximity to each other is examined next. Stratigraphic layering for snow sample 6 (Figure 24) is constructed by superimposing the layering of samples 4 and 5.

Higher thermal conductivity associated with the more dense snow layers causes warmer temperatures to be maintained from the base of the sample through the upper dense layer. As demonstrated previously, higher supersaturations are sustained at warmer temperatures. Above the upper high density layer, the temperature drops off very rapidly as the top surface is approached (Figure 25). This sharp change in temperature results in the large negative temperature gradient which exists in the uppermost zone of the sample (Figure 26).

A combination of the increase of the excess vapor density above the lower dense snow layer and below the upper dense snow layer causes a large excess vapor density to be produced in the low density snow between these layers (Figure 27). This effect is heavily increased by the large negative temperature gradient and relatively warm temperatures involved in this zone. It is also the large negative temperature gradient and warm temperature which causes the pronounced spike in the excess vapor density profile just above the upper high density snow layer. Since excess vapor density governs the growth of depth hoar, it may be assumed that when a low density snow is sandwiched between two higher density layers, at sufficiently warm temperatures, faceted crystal growth will be enhanced between and above the layers.

Depth hoar development associated with high density layers is of particular interest in avalanche stability evaluation. High density snow is quite often well sintered, resulting in a layer of high strength. Although not accounted for in the formulation, well sintered snow

is assumed to have a higher conductivity than a poorly bonded snow of the same density. A well bonded layer will further increase the effects of high density layering. In fact, sintering alone, with no increase in snow density, will quite likely have a similar effect as densification on the thermal regime of the snowpack.

Any hard flat layer of snow in a pack may provide an excellent surface on which snow can slide, and these layers are very frequently associated with avalanche occurrence. When a hard sliding surface exists in conjunction with even a thin layer of depth hoar immediately above or below the crust, the avalanche problem is compounded. Once the fragile bonds associated with depth hoar are broken, because of the added weight of new snow, impact or any other appropriate stress, the individual ice crystals form a relatively cohesionless layer. The loose faceted crystals will act as a lubricating agent, assisting the flow of snow on the sliding plane. If, as indicated theoretically, depth hoar growth is enhanced between two layers of high density snow, the likelihood of avalanche occurrence is increased, when several layers of dense snow are interspersed with low density snow. Two smooth sliding surfaces with a lubricating layer between must certainly encourage snowpack instability.

Initial grain size of a snow sample is also shown to have an effect. Snow with grains which have a smaller radius of curvature will also have a smaller pore space than a pack with larger grains but of the same density (Equation 34). All of the samples examined to this point have a mean radius of curvature of 0.0005 m. Round grains for sample 7 have a mean radius of 0.0001 m. The effect which this has is shown by comparison of Figures 27 and 28. The maximum excess vapor density curves for the two samples are essentially the same, but the values are lower for the smaller grained snow. Fine grained snow also has a

smaller magnitude of negative excess vapor density at the bottom of the pore. Compare Tables 5 and 6. These results indicate that fine grained snow will be less susceptible to depth hoar development than coarse grained snow of equal density, because of the correlation of the grain size to the pore size.

Finally, three test cases are examined for which the geometry and temperature conditions are specified. Akitaya (1974) cut cylindrical holes 0.008 m in diameter from fine grained compact snow. The grain size ranged from 0.0005 to 0.0010 m. Temperatures at the center of each of the three holes were 268.06°K, 269.26°K and 270.96°K. Each hole was subjected to a temperature gradient of 92 $deg \cdot m^{-1}$. The crystal habit of the depth hoar which developed in the space was then examined.

Making use of the specified conditions, using a mean radius of curvature of 0.00075 m, an analysis of the vapor pressure in the holes is carried out by using the formulation of Chapter IV. The temperature and maximum excess vapor density at the top of the pore is calculated and compared to the results observed for crystals grown in the atmosphere (Kobayashi, 1961, Figure 2).

Crystal habit development using values for excess vapor density obtained for the model, and applied to Kobayashi's empirical results are in generally good agreement with the actual crystals which were produced in Akitaya's experiment. The results are summarized in Table 7. Of the three holes, two produced exactly the crystal types predicted by the model, for the given conditions. Development in the hole with a center temperature of 269.26°K differed from that predicted theoretically. The excess vapor density given by the model for this example is slightly higher than that which would yield cups according to Kobayashi's diagram (Figure 2). It should be noted, however, that the type

of crystal which would be expected to develop, based on temperature and temperature gradient, in accordance with Akitaya's diagram (Figure 1) would also yield needles instead of cups.

The correlation between the type of crystals grown in the atmosphere and those grown in snow (when the exact pore and crystal geometry is known) is significant. It indicates that excess vapor density of a similar magnitude to those which govern the secondary growth features of ice crystals in air, may also be present in snow.

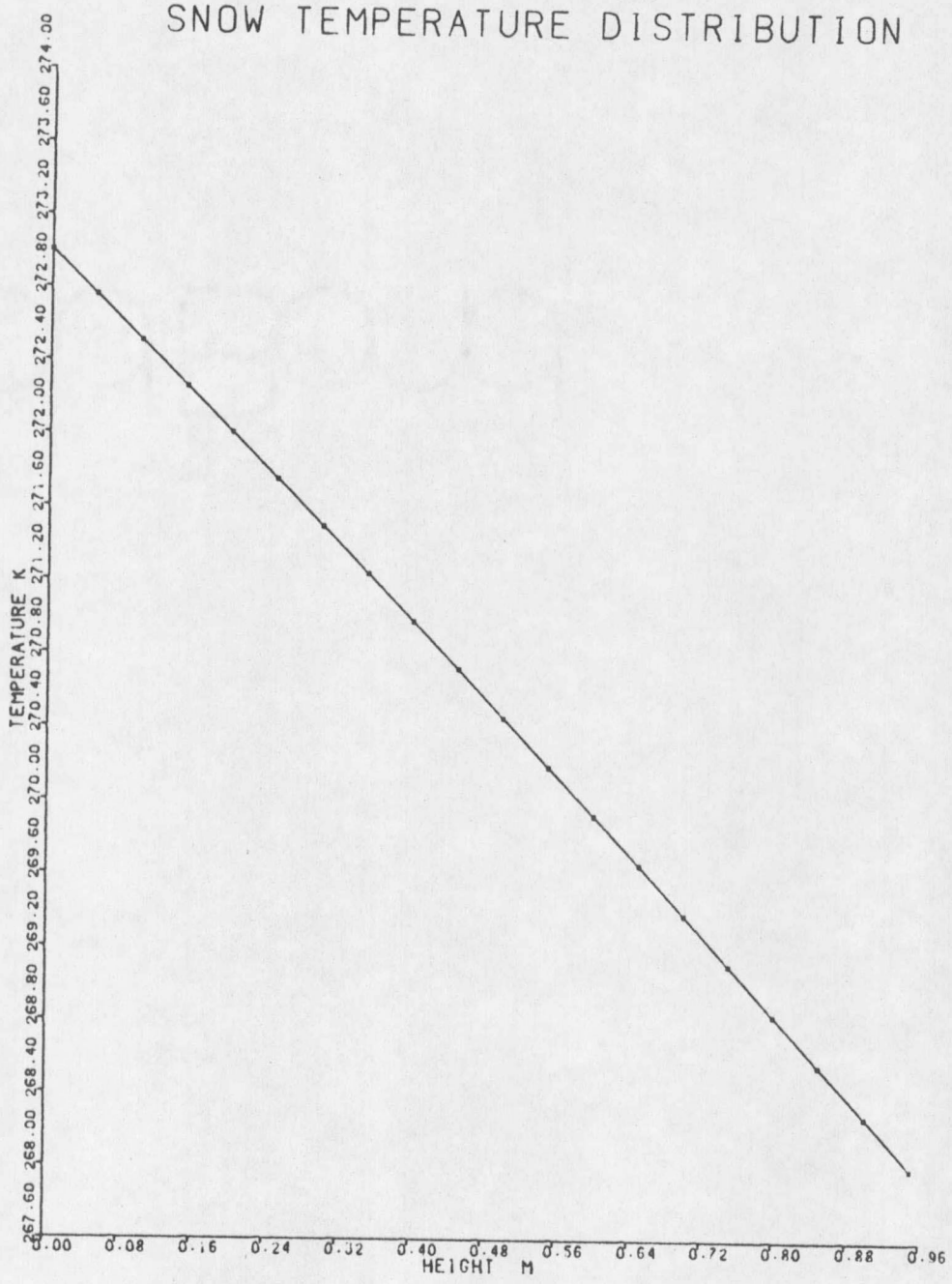

Figure 5. Temperature Profile for Homogeneous Density Snow of 200 KG-M^{-3} (Sample 1), Which Has Temperature Difference of 5°K Between the Top and Bottom Boundaries.

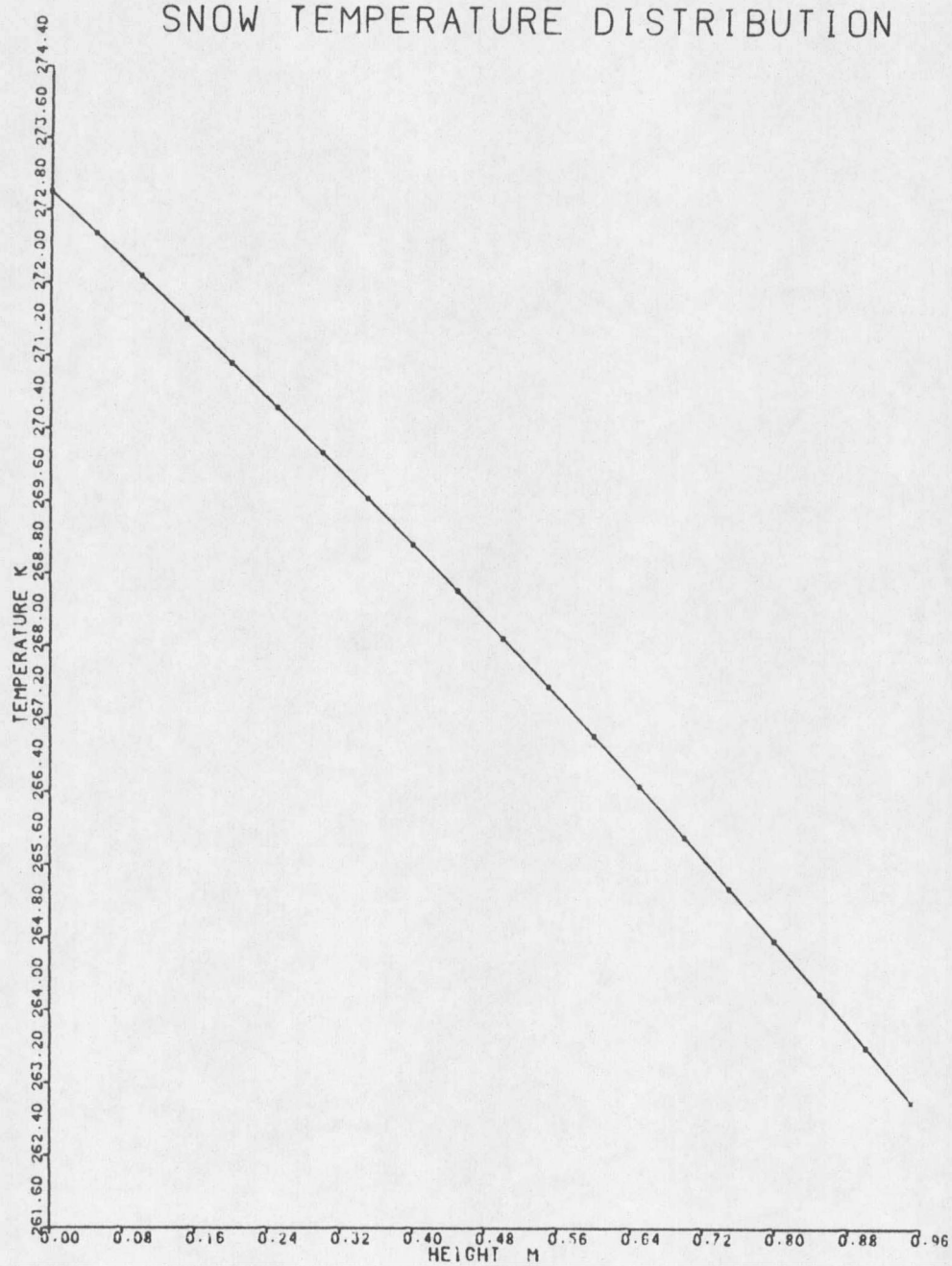

Figure 6. Temperature Profile for Homogeneous Density Snow of 200 KG-M^{-3} (Sample 1), Which Has Temperature Difference of 10°K Between the Top and Bottom Boundaries.

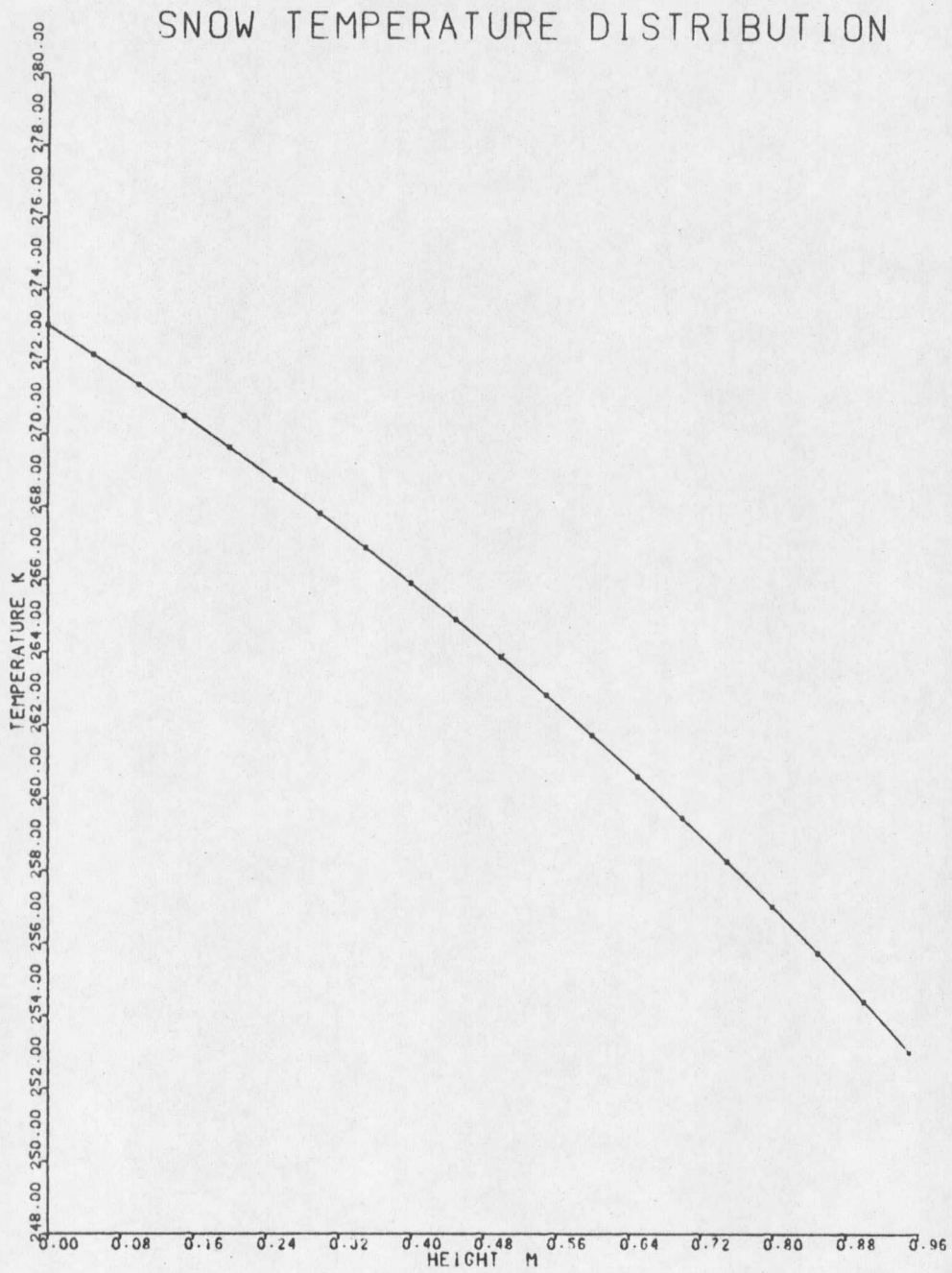

Figure 7. Temperature Profile for Homogeneous Density Snow of 200 KG-M^{-3} (Sample 1), Which Has Temperature Difference of 20°K Between the Top and Bottom Boundaries.

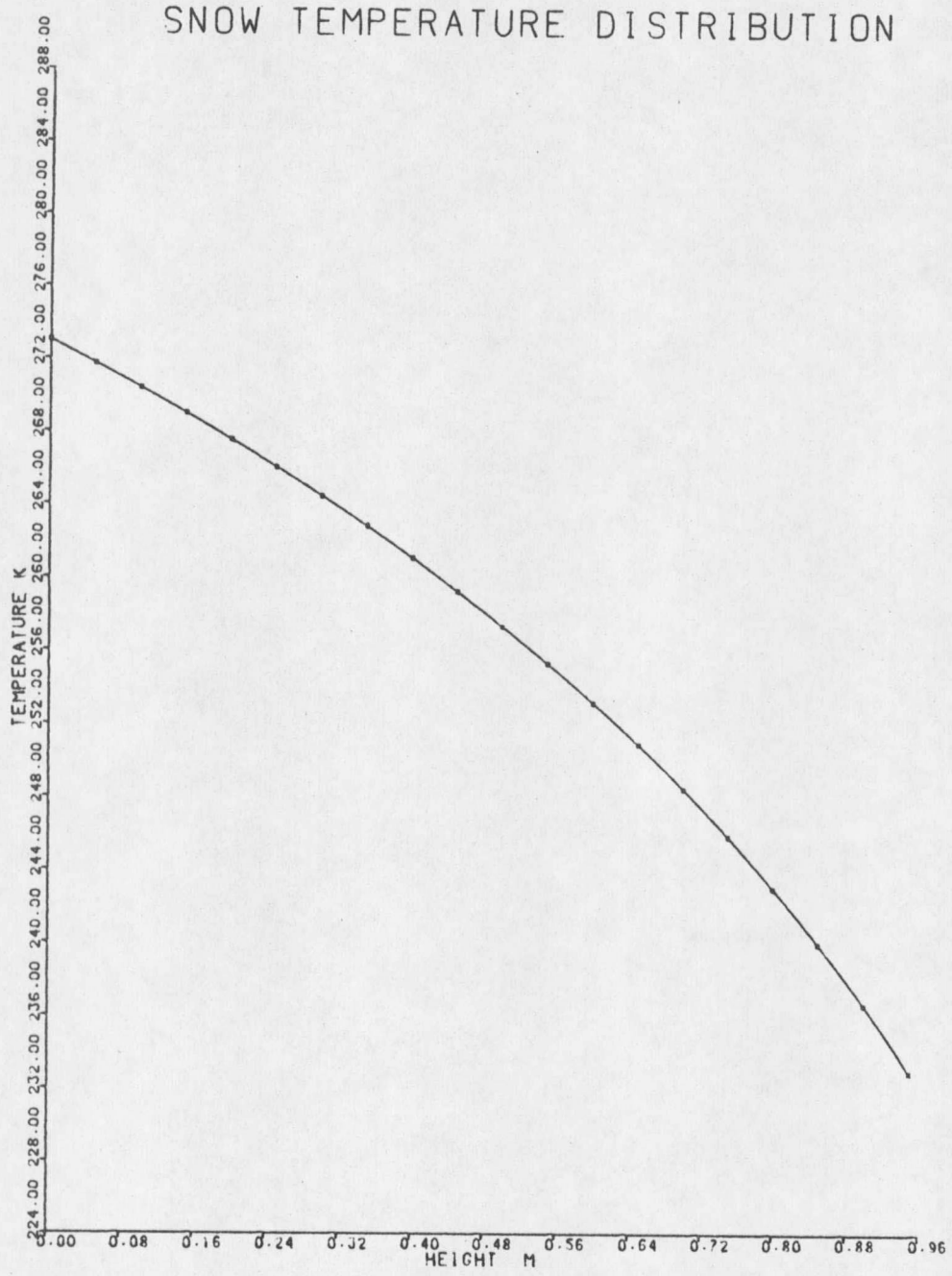

Figure 8. Temperature Profile for Homogeneous Density Snow of 200 KG-M^{-3} (Sample 1), Which Has Temperature Difference of 40°K Between the Top and Bottom Boundaries.

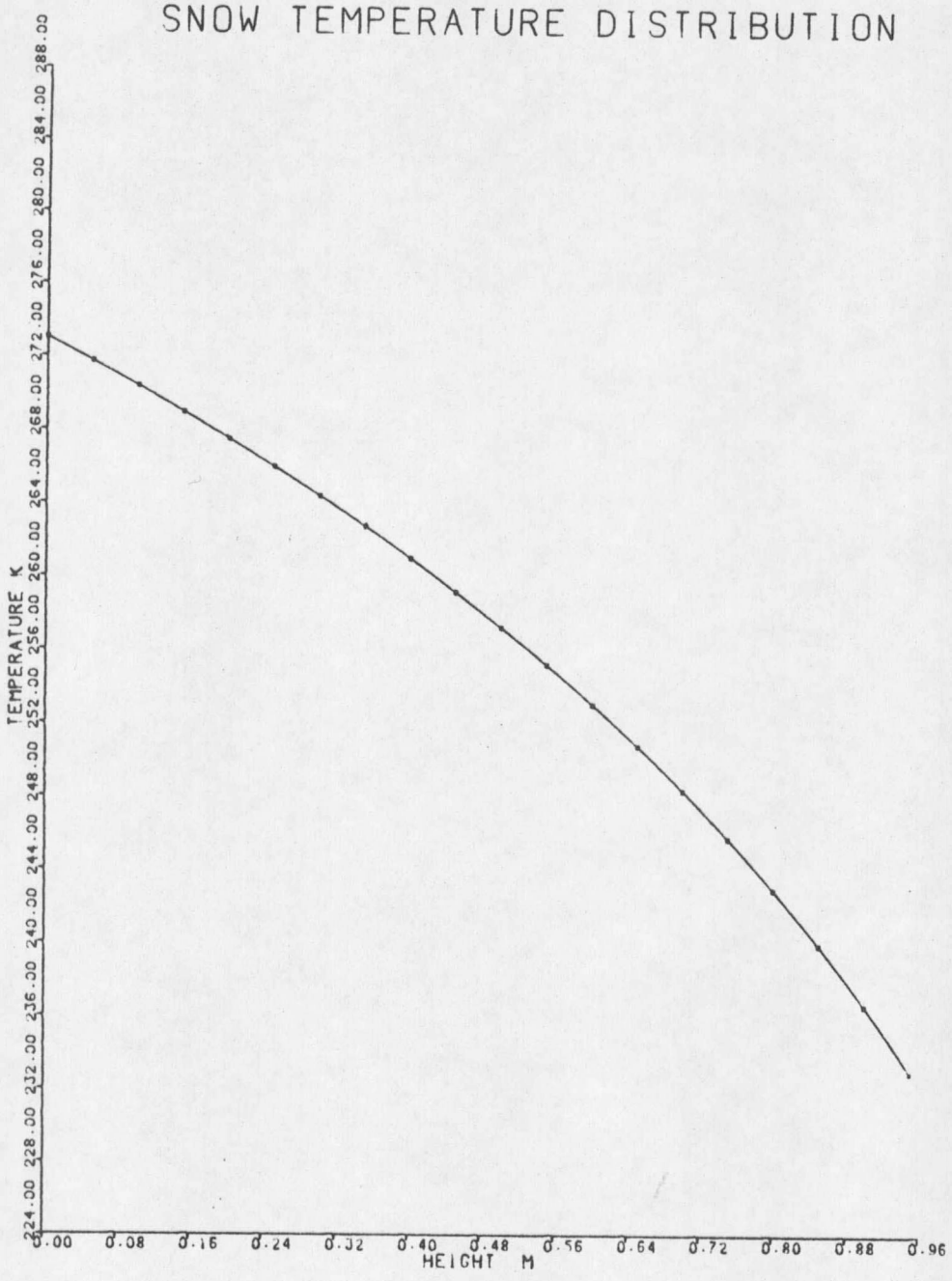

Figure 9. Temperature Profile for Homogeneous Density Snow of 100 KG-M^{-3} (Sample 2), Which Has Temperature Difference of 40°K Between the Top and Bottom Boundaries.

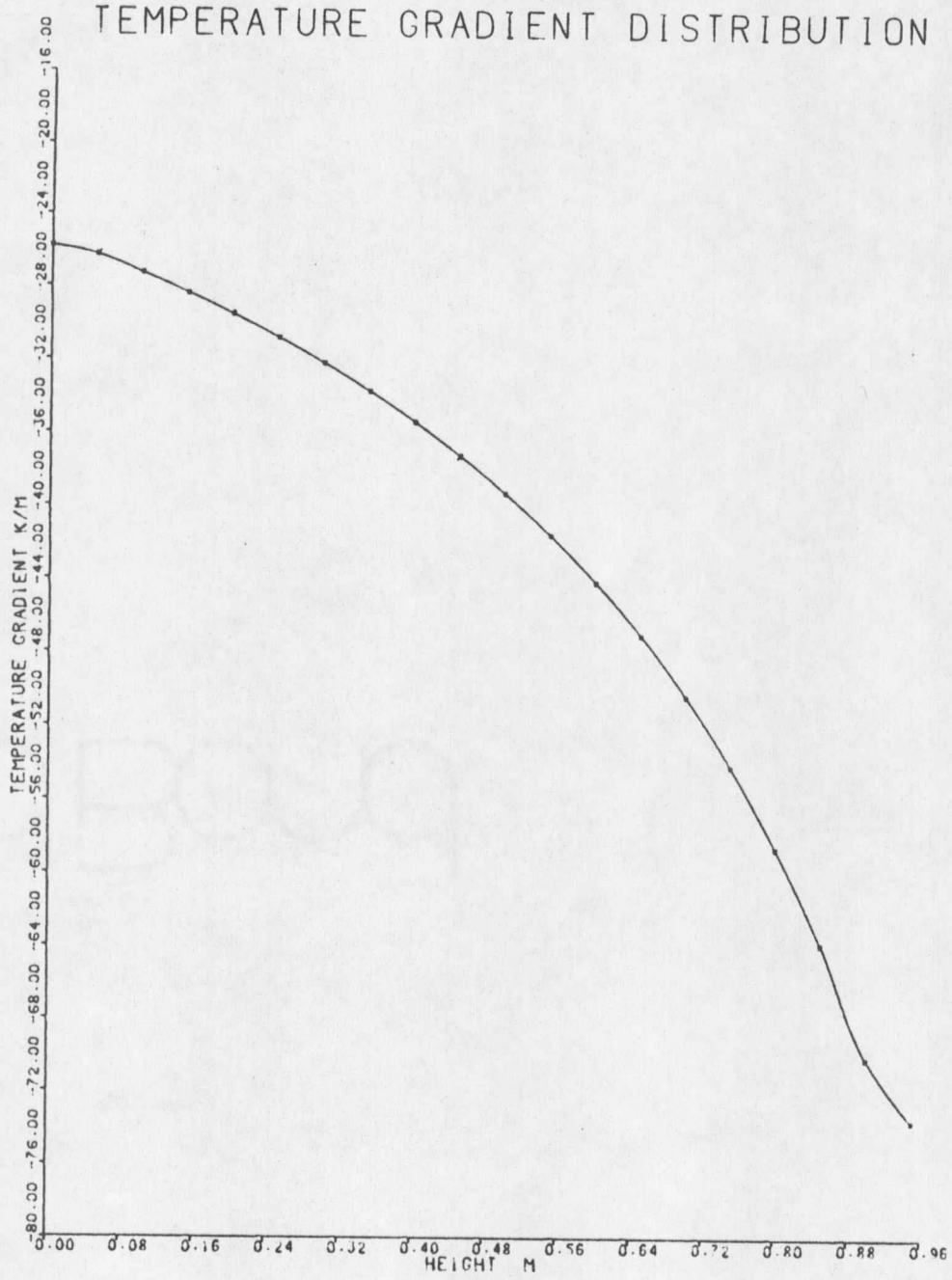

Figure 10. Temperature Gradient Profile For Snow Sample 2.

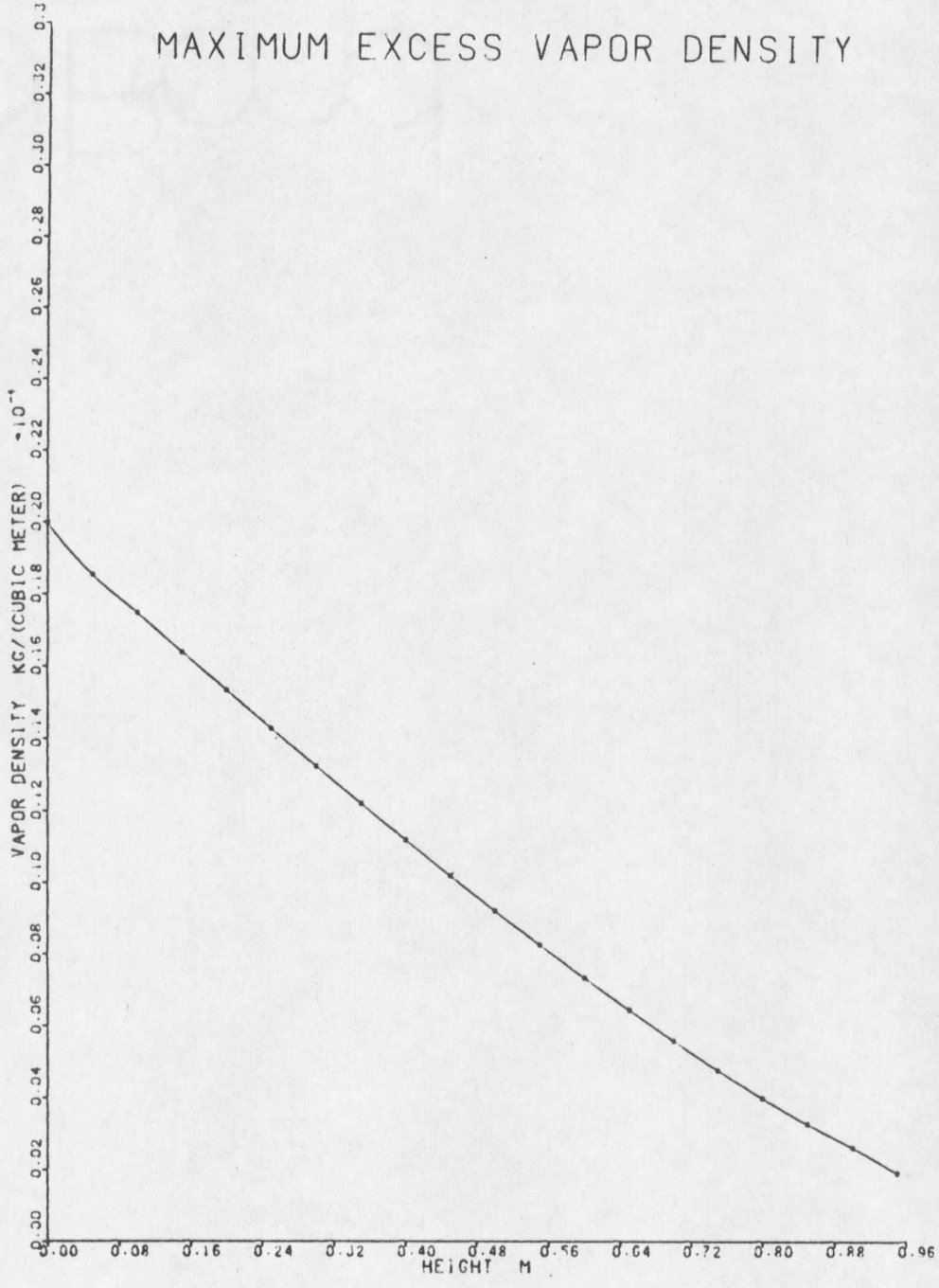

Figure 11. Excess Vapor Density at the Top of the Pore Space Over Flat Surfaced Crystals in Snow Sample 2.

Table 1. Detailed Summary of the Analysis Results for the Pore Space at Each Node, for Snow Sample 2.

Height	Temperature °K	Temperature Gradient Deg m^{-1}	Snow Density $KG \cdot m^{-3}$	Pore Height m	Pore Pressure PA	Excess Vapor Density $KG \cdot m^{-3} \times 10^{-5}$					
						Bottom of the Pore			Top of the Pore		
						Over Neck	Over Round Surface	Over Flat Surface	Over Neck	Over Round Surface	Over Flat Surface
0.00	273.00	-25.82	100	0.0039	600.49	-2.0010	-1.9938	-1.9920	1.9890	1.9961	1.9979
0.05	271.71	-26.30	100	0.0039	539.56	-1.8579	-1.8514	-1.8498	1.8464	1.8528	1.8544
0.10	270.37	-27.31	100	0.0039	482.36	-1.7495	-1.7436	-1.7422	1.7404	1.7462	1.7477
0.15	268.98	-28.39	100	0.0039	428.83	-1.6416	-1.6364	-1.6351	1.6330	1.6382	1.6395
0.20	267.53	-29.56	100	0.0039	378.95	-1.5354	-1.5307	-1.5296	1.5278	1.5324	1.5335
0.25	266.02	-30.84	100	0.0039	332.65	-1.4296	-1.4256	-1.4245	1.4230	1.4271	1.4281
0.30	264.44	-32.23	100	0.0039	289.87	-1.3246	-1.3211	-1.3201	1.3193	1.3228	1.3237
0.35	262.80	-33.75	100	0.0039	250.56	-1.2214	-1.2182	-1.2175	1.2172	1.2203	1.2211
0.40	261.07	-35.42	100	0.0039	214.64	-1.1204	-1.1177	-1.1170	1.1162	1.1189	1.1196
0.45	259.26	-37.26	100	0.0039	182.03	-1.0208	-1.0185	-1.0179	1.0171	1.0194	1.0199
0.50	257.35	-39.30	100	0.0039	152.64	-0.9227	-0.9208	-0.9203	0.9199	0.9218	0.9223
0.55	255.33	-41.59	100	0.0039	126.37	-0.8277	-0.8261	-0.8256	0.8252	0.8268	0.8272
0.60	253.19	-44.15	100	0.0039	103.10	-0.7352	-0.7338	-0.7335	0.7332	0.7345	0.7348
0.65	250.91	-47.05	100	0.0039	82.73	-0.6457	-0.6446	-0.6443	0.6444	0.6455	0.6457
0.70	248.48	-50.36	100	0.0039	65.11	-0.5600	-0.5591	-0.5589	0.5589	0.5598	0.5600
0.75	245.88	-54.18	100	0.0039	50.09	-0.4782	-0.4776	-0.4774	0.4775	0.4782	0.4783
0.80	243.06	-58.62	100	0.0039	37.51	-0.4010	-0.4005	-0.4004	0.4006	0.4011	0.4012
0.85	240.01	-63.86	100	0.0039	27.20	-0.3289	-0.3286	-0.3285	0.3287	0.3290	0.3291
0.90	236.68	-70.14	100	0.0039	18.96	-0.2626	-0.2623	-0.2622	0.2624	0.2627	0.2628
0.95	233.00	-73.57	100	0.0039	12.58	-0.1915	-0.1914	-0.1913	0.1915	0.1917	0.1918

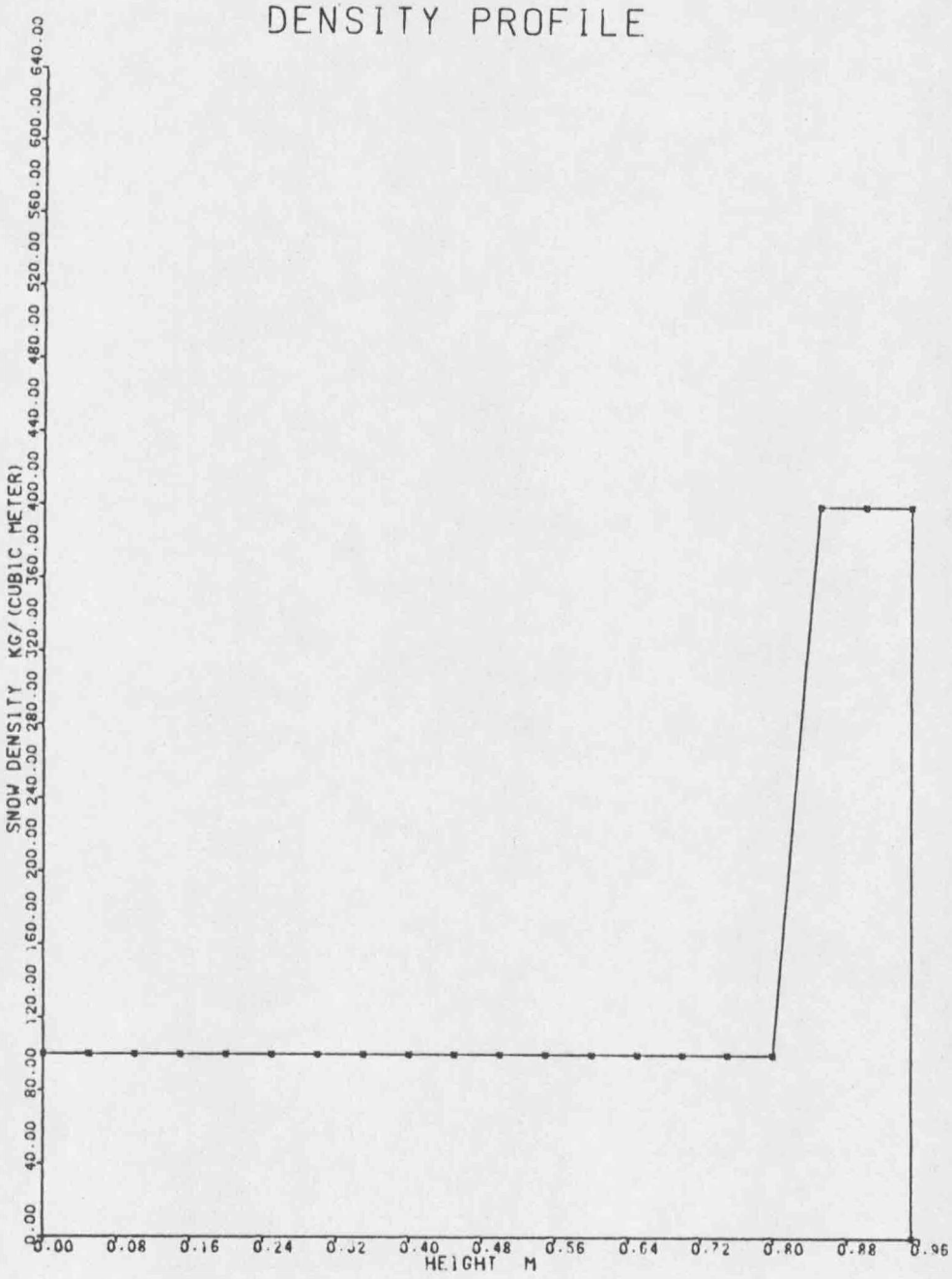

Figure 12. Density Profile for Snow Sample 3.

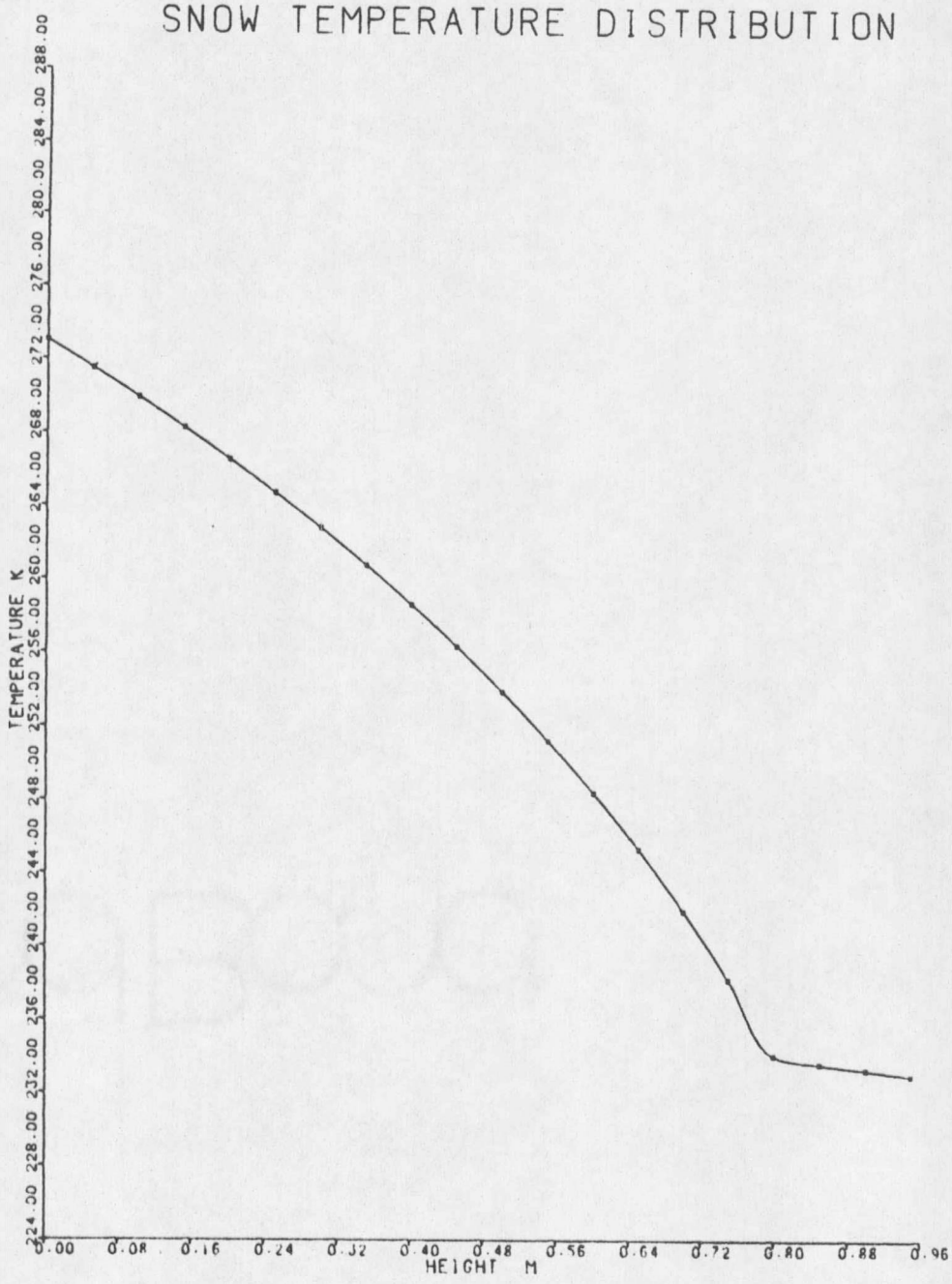

Figure 13. Temperature Profile for Snow Sample 3.

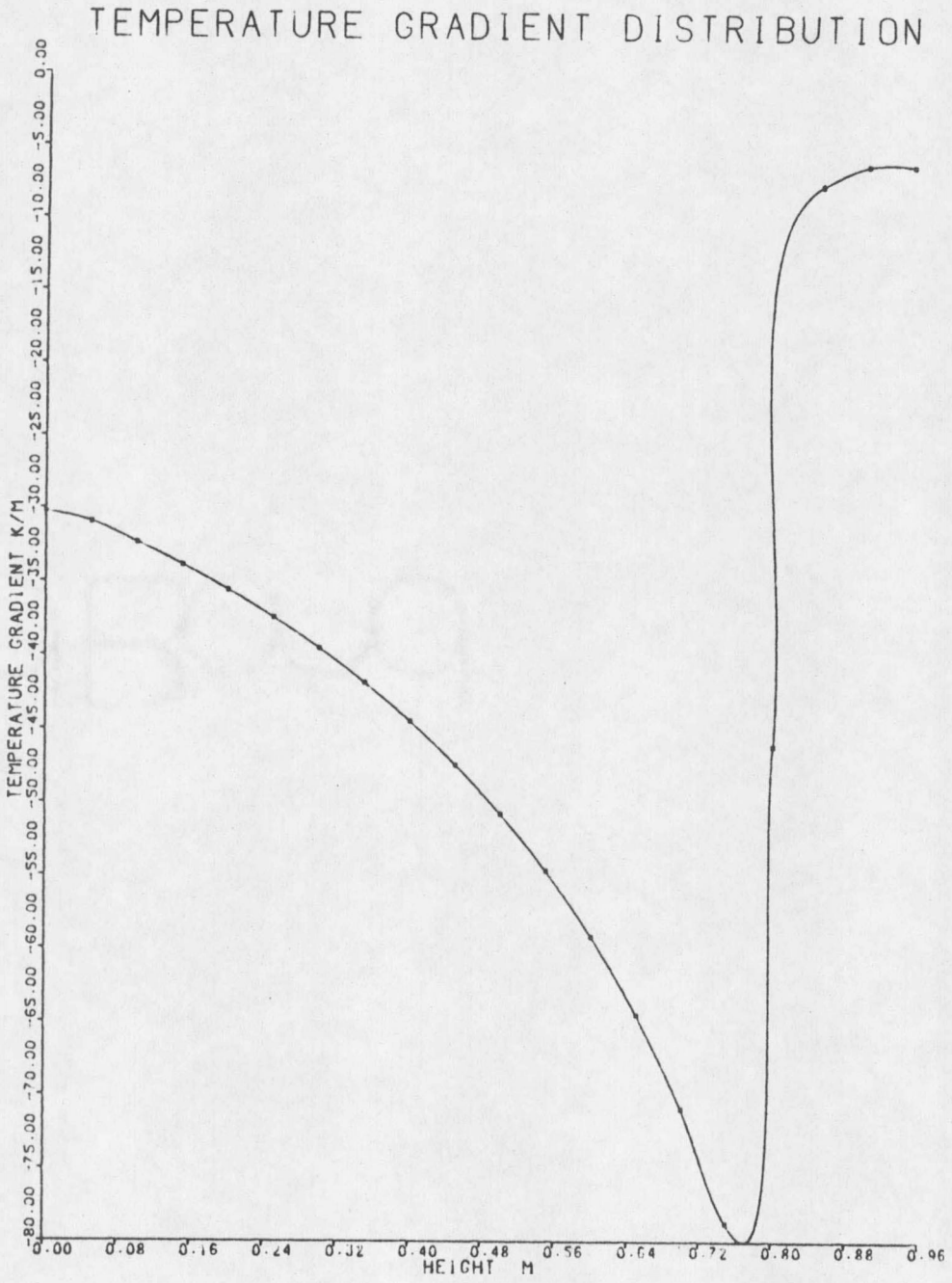

Figure 14. Temperature Gradient Profile for Snow Sample 3.

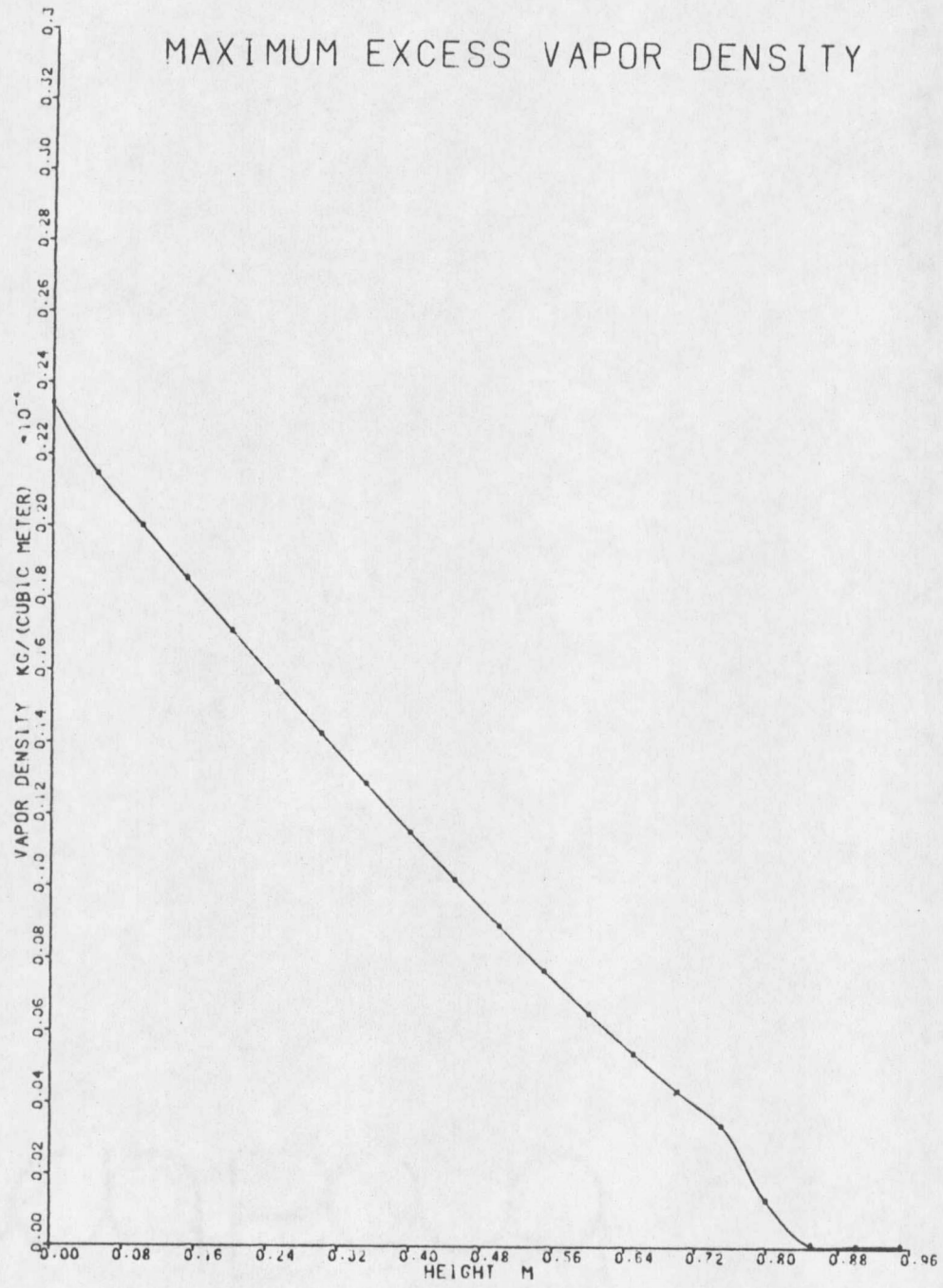

Figure 15. Excess Vapor Density at the Top of the Pore Space Over Flat Surfaced Crystals in Snow Sample 3.

Table 2. Detailed Summary of the Analysis Results for the Pore Space at Each Node, for Snow Sample 3.

Height	Temperature °K	Temperature Gradient Deg m^{-1}	Snow Density $KG \cdot m^{-3}$	Pore Height m	Pore Pressure PA	Excess Vapor Density $KG \cdot m^{-3} \times 10^{-5}$					
						Bottom of the Pore			Top of the Pore		
						Over Neck	Over Round Surface	Over Flat Surface	Over Neck	Over Round Surface	Over Flat Surface
0.00	273.00	-30.28	100	0.0039	600.49	-2.3455	-2.3383	-2.3365	2.3329	2.3400	2.3418
0.05	271.49	-30.95	100	0.0039	529.63	-2.1497	-2.1433	-2.1417	2.1385	2.1449	2.1465
0.10	269.90	-32.35	100	0.0039	463.84	-2.0024	-1.9968	-1.9954	1.9940	1.9996	2.0010
0.15	268.25	-33.89	100	0.0039	403.06	-1.8555	-1.8506	-1.8493	1.8482	1.8531	1.8543
0.20	266.52	-35.57	100	0.0039	347.22	-1.7110	-1.7067	-1.7056	1.7048	1.7090	1.7101
0.25	264.69	-37.44	100	0.0039	296.23	-1.5679	-1.5642	-1.5633	1.5626	1.5663	1.5672
0.30	262.77	-39.51	100	0.0039	249.98	-1.4268	-1.4237	-1.4229	1.4222	1.4253	1.4261
0.35	260.74	-41.82	100	0.0039	208.36	-1.2882	-1.2856	-1.2849	1.2847	1.2873	1.2879
0.40	258.59	-44.42	100	0.0039	171.24	-1.1530	-1.1508	-1.1503	1.1500	1.1521	1.1526
0.45	259.30	-47.37	100	0.0039	138.47	-1.0209	-1.0191	-1.0187	1.0187	1.0205	1.0209
0.50	253.85	-50.73	100	0.0039	109.89	-0.8931	-0.8916	-0.8913	0.8911	0.8925	0.8929
0.55	251.23	-54.61	100	0.0039	85.32	-0.7699	-0.7688	-0.7685	0.7685	0.7696	0.7698
0.60	248.39	-59.14	100	0.0039	64.53	-0.6522	-0.6514	-0.6511	0.6514	0.6522	0.6524
0.65	245.31	-64.48	100	0.0039	47.30	-0.5410	-0.5404	-0.5402	0.5406	0.5412	0.5413
0.70	241.94	-70.89	100	0.0039	33.37	-0.4373	-0.4368	-0.4367	0.4371	0.4375	0.4376
0.75	238.22	-78.71	100	0.0039	22.44	-0.3420	-0.3417	-0.3416	0.3420	0.3423	0.3424
0.80	234.07	-46.05	100	0.0039	14.20	-0.1336	-0.1334	-0.1333	0.1333	0.1335	0.1336
0.85	233.62	- 7.62	400	0.0016	13.50	-0.0088	-0.0086	-0.0085	0.0084	0.0085	0.0086
0.90	233.31	- 6.20	400	0.0016	13.03	-0.0070	-0.0068	-0.0067	0.0065	0.0067	0.0068
0.95	233.00	- 6.22	400	0.0016	12.58	-0.0068	-0.0066	-0.0065	0.0064	0.0065	0.0066

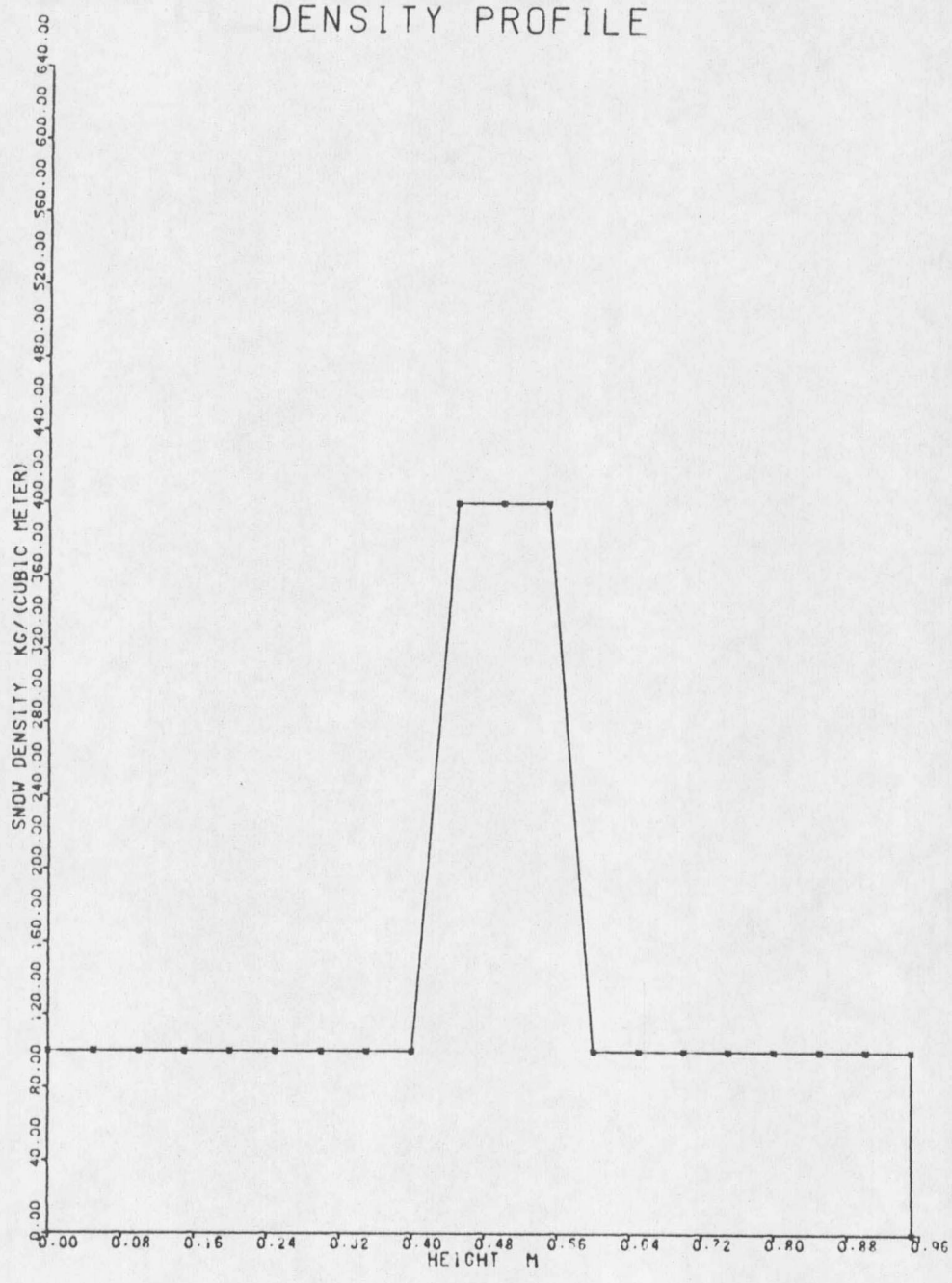

Figure 16. Density Profile For Snow Sample 4.

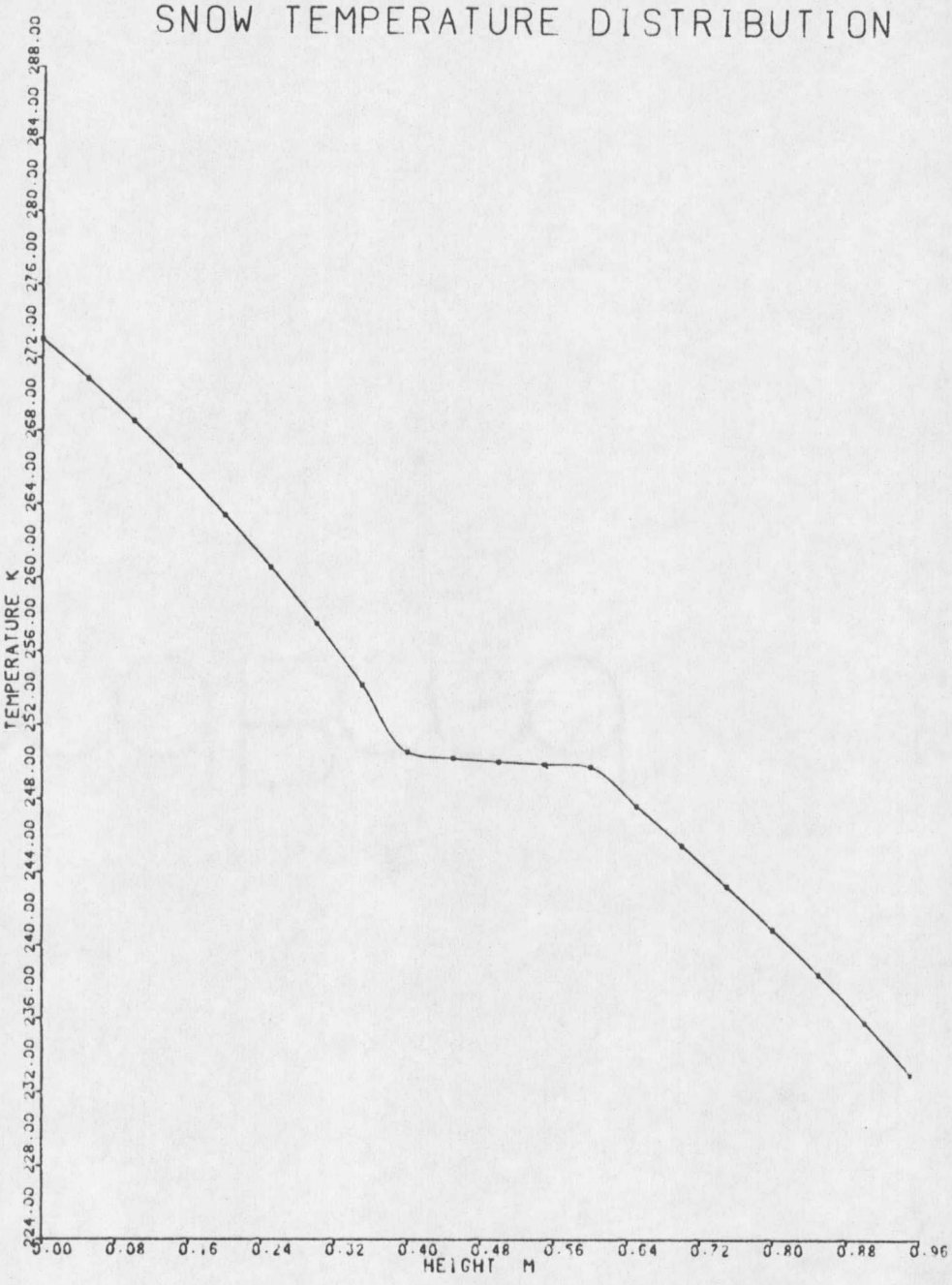

Figure 17. Temperature Profile For Snow Sample 4.

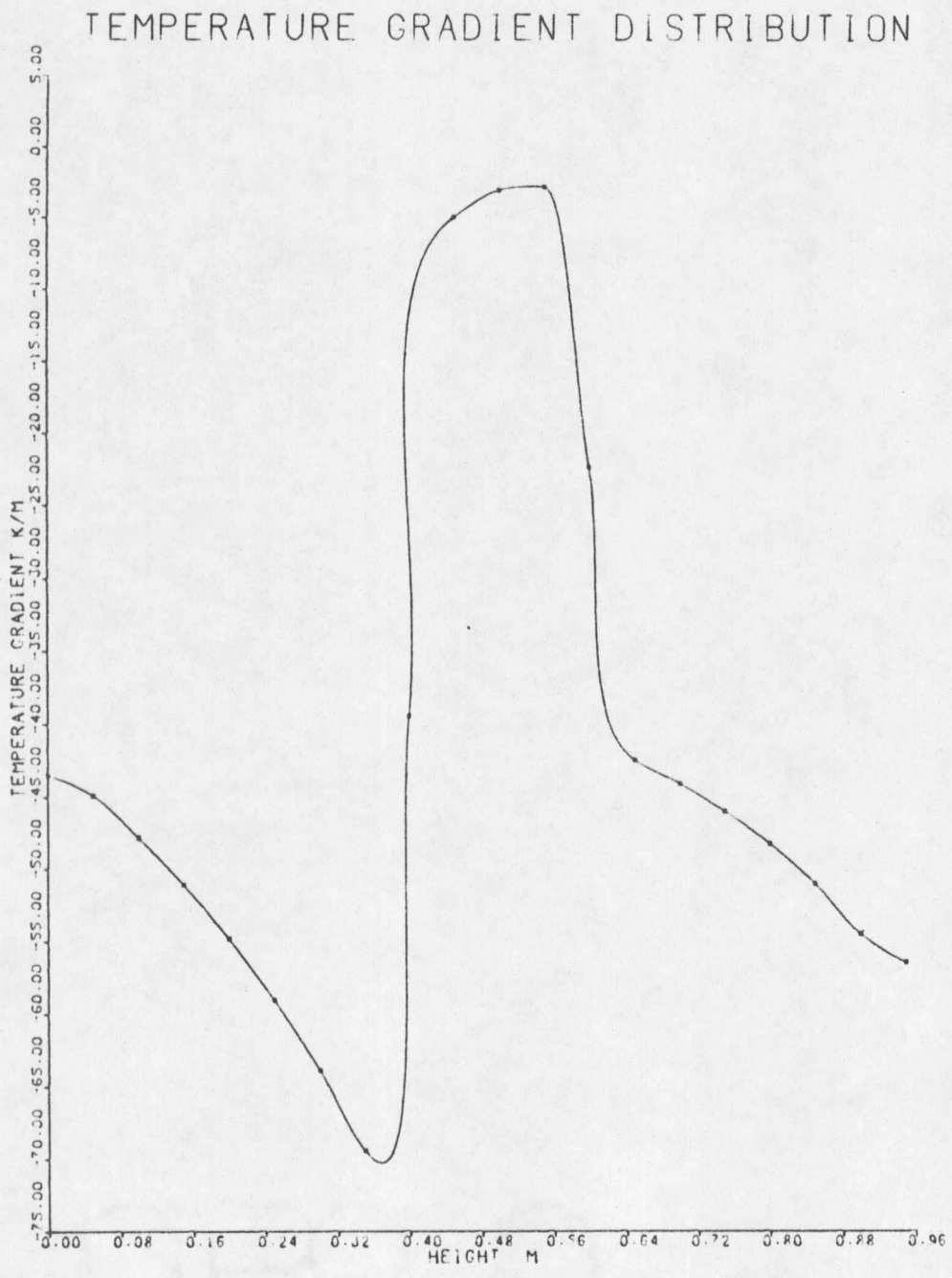

Figure 18. Temperature Gradient Profile For Snow Sample 4.

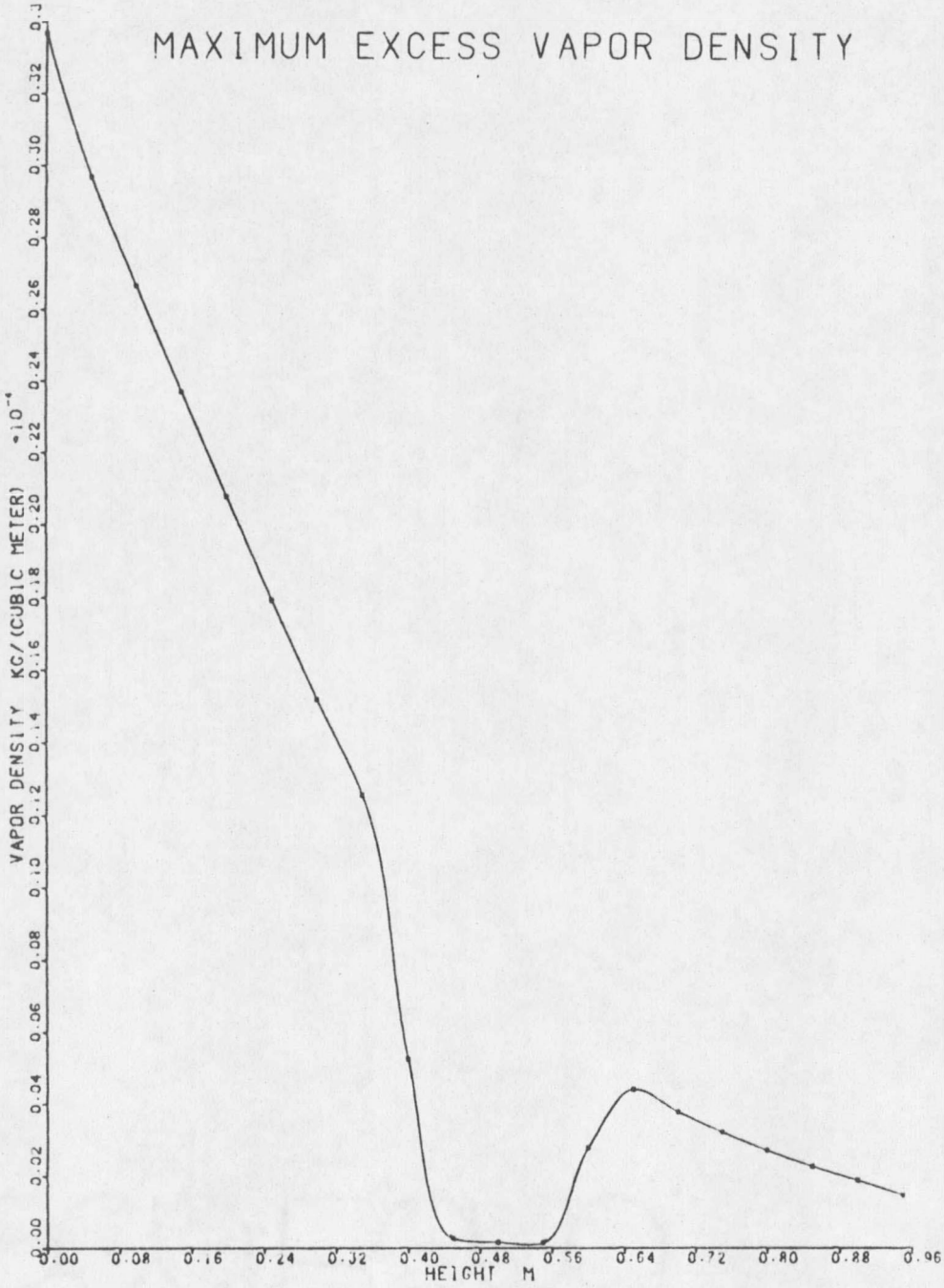

Figure 19. Excess Vapor Density at the Top of the Pore Space Over Flat Surfaced Crystals in Snow Sample 4.

Table 3. Detailed Summary of the Analysis Results for the Pore Space at Each Node, for Snow Sample 4.

Height	Temperature °K	Temperature Gradient Deg m^{-1}	Snow Density $KG \cdot m^{-3}$	Pore Height m	Pore Pressure PA	Excess Vapor Density $KG \cdot m^{-3} \times 10^{-5}$					
						Bottom of the Pore			Top of the Pore		
						Over Neck	Over Round Surface	Over Flat Surface	Over Neck	Over Round Surface	Over Flat Surface
0.00	273.00	-43.53	100	0.0039	600.50	-3.3687	-3.3615	-3.3597	3.3580	3.3652	3.3670
0.05	270.82	-44.90	100	0.0039	501.10	-2.9695	-2.9634	-2.9619	2.9607	2.9666	2.9681
0.10	268.51	-47.80	100	0.0039	412.10	-2.6673	-2.6623	-2.6610	2.6602	2.6652	2.6664
0.15	266.04	-51.08	100	0.0039	333.28	-2.3690	-2.3649	-2.3639	2.3640	2.3680	2.3690
0.20	263.40	-54.80	100	0.0039	264.35	-2.0770	-2.0738	-2.0729	2.0733	2.0766	2.0774
0.25	260.56	-59.03	100	0.0039	205.00	-1.7920	-1.7894	-1.7887	1.7891	1.7916	1.7922
0.30	257.50	-63.87	100	0.0039	154.82	-1.5169	-1.5149	-1.5144	1.5152	1.5171	1.5176
0.35	254.18	-69.42	100	0.0039	113.32	-1.2544	-1.2529	-1.2525	1.2535	1.2549	1.2553
0.40	250.56	-39.45	100	0.0039	79.91	-0.5253	-0.5243	-0.5240	0.5237	0.5248	0.5250
0.45	250.23	- 5.01	400	0.0016	77.40	-0.0272	-0.0263	-0.0260	0.0254	0.0264	0.0267
0.50	250.56	- 3.07	400	0.0016	76.07	-0.0169	-0.0159	-0.0156	0.0150	0.0160	0.0162
0.55	249.92	- 2.85	400	0.0016	75.09	-0.0156	-0.0147	-0.0144	0.0136	0.0146	0.0148
0.60	249.77	-22.38	100	0.0039	73.97	-0.2791	-0.2781	-0.2778	0.2772	0.2782	0.2784
0.65	247.69	-42.47	100	0.0039	60.13	-0.4404	-0.4394	-0.4396	0.4393	0.4401	0.4403
0.70	245.52	-44.10	100	0.0039	48.33	-0.3774	-0.3768	-0.3766	0.3764	0.3771	0.3772
0.75	243.28	-45.99	100	0.0039	38.34	-0.3210	-0.3204	-0.3203	0.3203	0.3208	0.3209
0.80	240.92	-48.25	100	0.0039	29.96	-0.2709	-0.2705	-0.2704	0.2704	0.2708	0.2709
0.85	238.45	-51.02	100	0.0039	22.99	-0.2267	-0.2264	-0.2263	0.2263	0.2266	0.2267
0.90	235.82	-54.50	100	0.0039	17.25	-0.1878	-0.1876	-0.1875	0.1876	0.1878	0.1879
0.95	233.00	-56.46	100	0.0039	12.58	-0.1471	-0.1469	-0.1468	0.1469	0.1470	0.1471

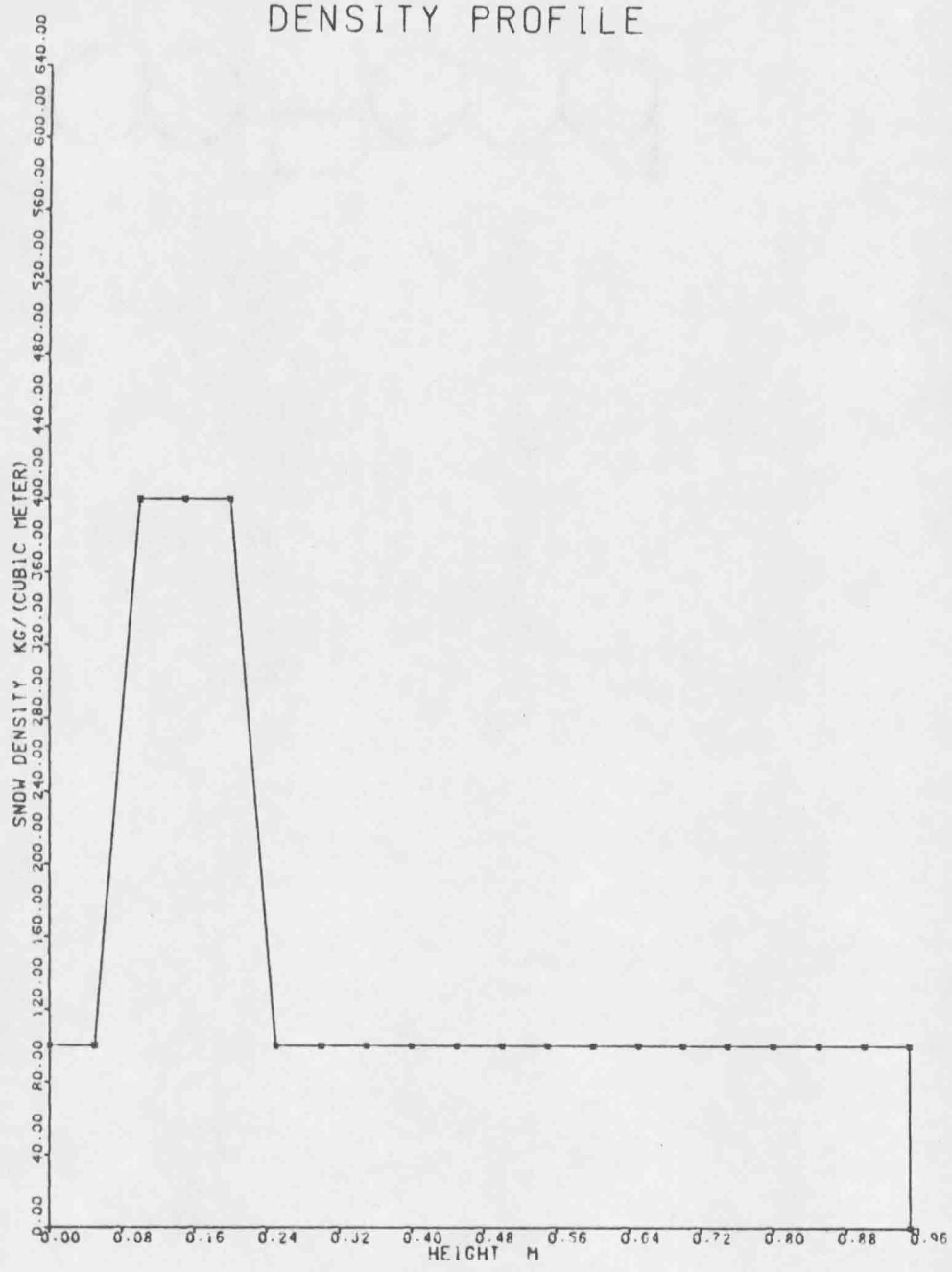

Figure 20. Density Profile For Snow Sample 5.

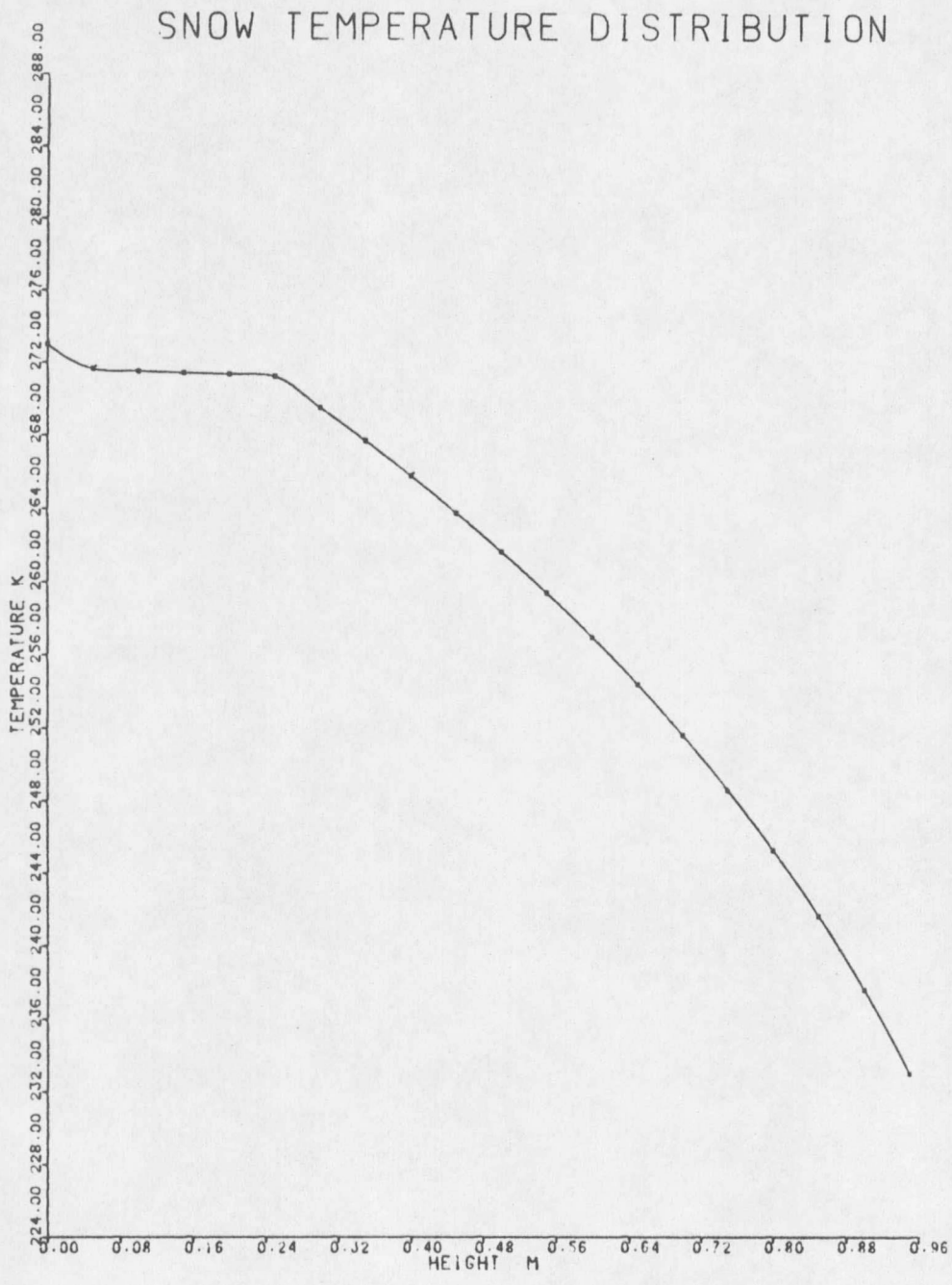

Figure 21. Temperature Profile For Snow Sample 5.

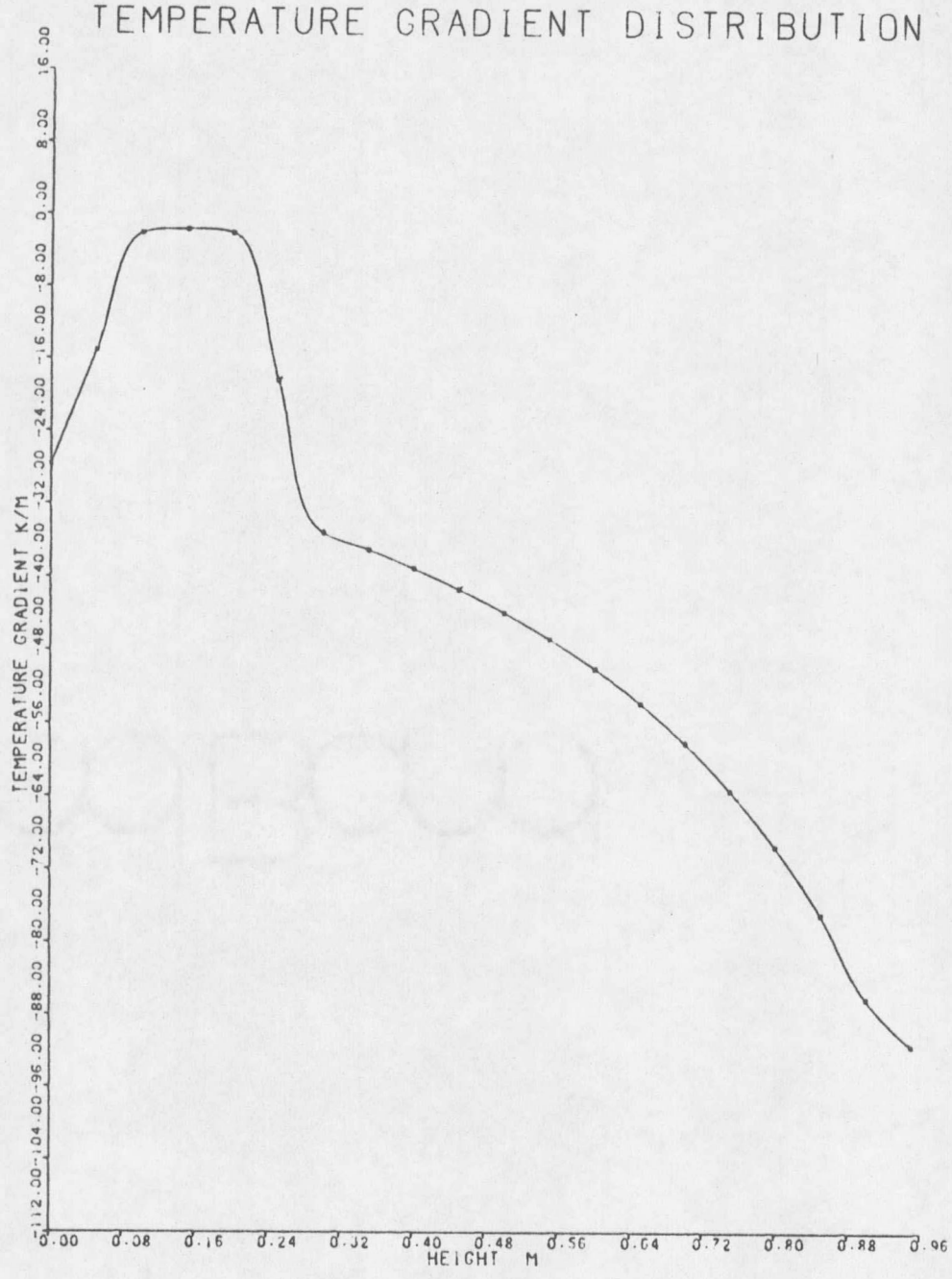

Figure 22. Temperature Gradient Profile For Snow Sample 5.

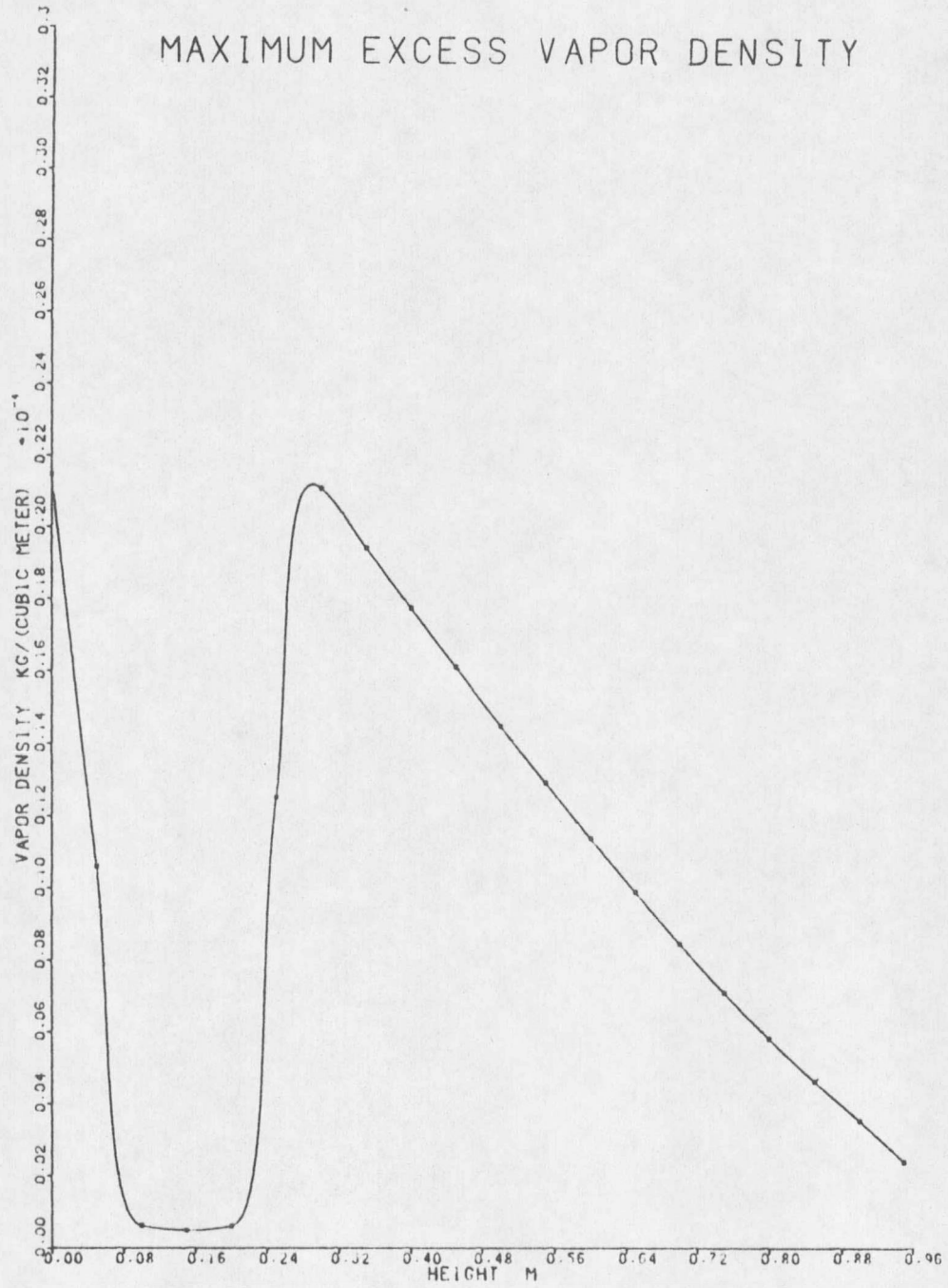

Figure 23. Excess Vapor Density at the Top of the Pore Space Over Flat Surfaced Crystals in Snow Sample 5.

Table 4. Detailed Summary of the Analysis Results for the Pore Space at Each Node, for Snow Sample 5.

Height	Temperature °K	Temperature Gradient Deg m^{-1}	Snow Density $KG \cdot m^{-3}$	Pore Height m	Pore Pressure PA	Excess Vapor Density $KG \cdot m^{-3} \times 10^{-5}$					
						Bottom of the Pore			Top of the Pore		
						Over Neck	Over Round Surface	Over Flat Surface	Over Neck	Over Round Surface	Over Flat Surface
0.00	273.00	-27.74	100	0.0039	600.49	-2.1497	-2.1425	-2.1407	2.1377	2.1449	2.1467
0.05	271.61	-15.13	100	0.0039	535.16	-1.0638	-1.0573	-1.0557	1.0518	1.0582	1.0598
0.10	271.49	- 2.11	400	0.0016	529.69	-0.0657	-0.0594	-0.0578	0.0537	0.0600	0.0616
0.15	271.40	- 1.70	400	0.0016	525.94	-0.0536	-0.0473	-0.0457	0.0416	0.0479	0.0495
0.20	271.32	- 2.109	400	0.0016	522.22	-0.0649	-0.0587	-0.0571	0.0530	0.0593	0.0609
0.25	271.19	-18.42	100	0.0039	516.76	-1.2563	-1.2501	-1.2485	1.2442	1.2504	1.2519
0.30	269.48	-35.21	100	0.0039	447.27	-2.1106	-2.1052	-2.1038	2.1014	2.1068	2.1082
0.35	267.67	-37.03	100	0.0039	383.55	-1.9423	-1.9376	-1.9364	1.9350	1.9396	1.9408
0.40	265.77	-39.05	100	0.0039	325.49	-1.7754	-1.7716	-1.7703	1.7692	1.7732	1.7742
0.45	263.77	-41.31	100	0.0039	272.99	-1.6110	-1.6076	-1.6067	1.6067	1.6101	1.6109
0.50	261.64	-43.85	100	0.0039	225.91	-1.4495	-1.4466	-1.4459	1.4458	1.4486	1.4493
0.55	259.38	-46.72	100	0.0039	184.10	-1.2915	-1.2892	-1.2886	1.2886	1.2909	1.2915
0.60	256.97	-49.99	100	0.0039	147.38	-1.1378	-1.1359	-1.1355	1.1354	1.1372	1.1377
0.65	254.39	-53.75	100	0.0039	115.56	-0.9886	-0.9871	-0.9867	0.9868	0.9883	0.9887
0.70	251.59	-58.13	100	0.0039	88.41	-0.8453	-0.8441	-0.8438	0.8440	0.8452	0.8454
0.75	248.57	-63.28	100	0.0039	65.67	-0.7088	-0.7079	-0.7079	0.7079	0.7087	0.7089
0.80	245.27	-69.45	100	0.0039	47.07	-0.5801	-0.5795	-0.5793	0.5796	0.5803	0.5804
0.85	241.63	-76.94	100	0.0039	32.26	-0.4606	-0.4602	-0.4601	0.4606	0.4610	0.4611
0.90	237.57	-86.25	100	0.0039	20.90	-0.3519	-0.3516	-0.3515	0.3520	0.3522	0.3523
0.95	233.00	-91.43	100	0.0039	12.58	-02380	-0.2378	-0.2377	0.2381	0.2381	0.2383

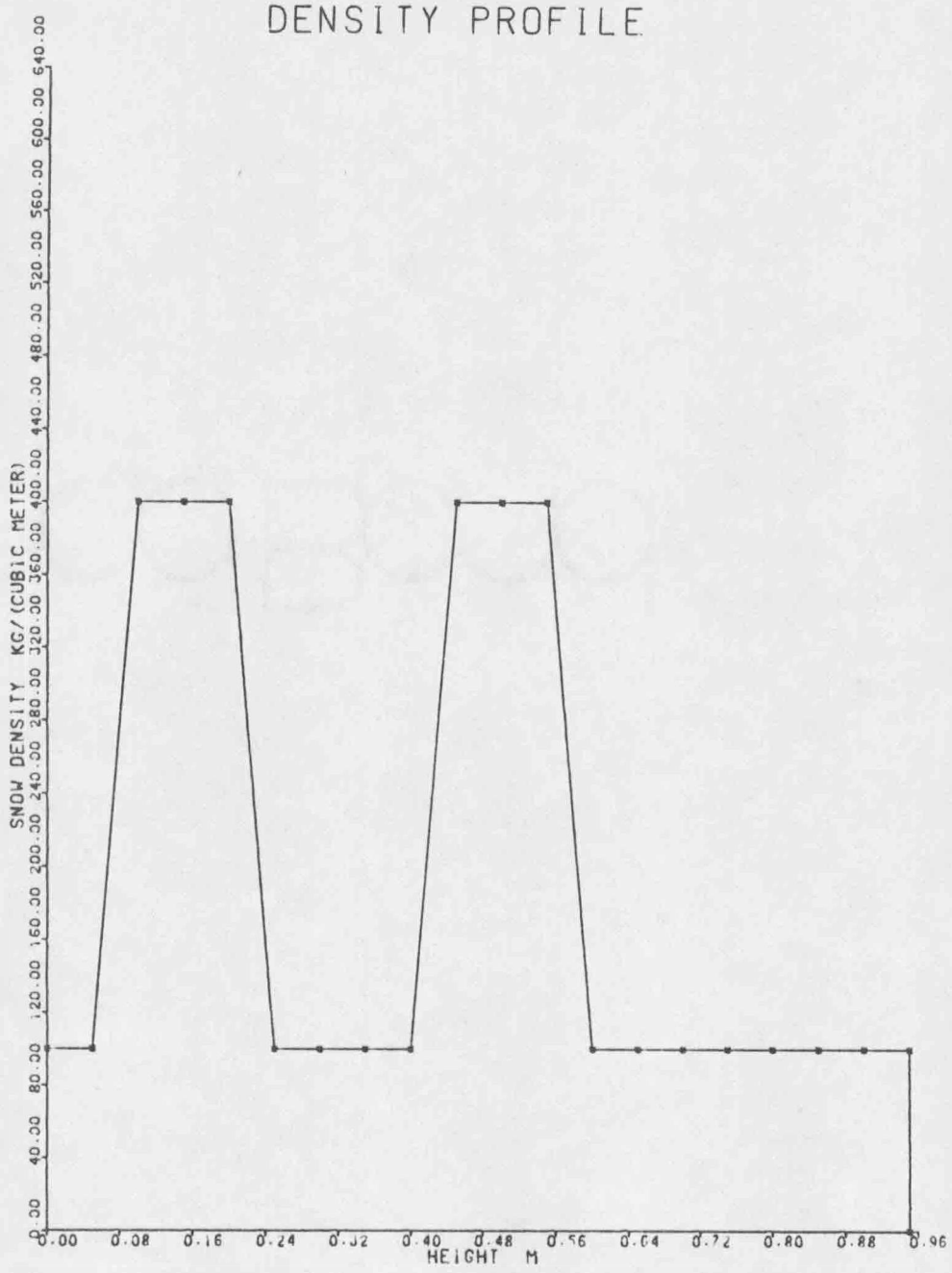

Figure 24. Density Profile For Snow Sample 6.

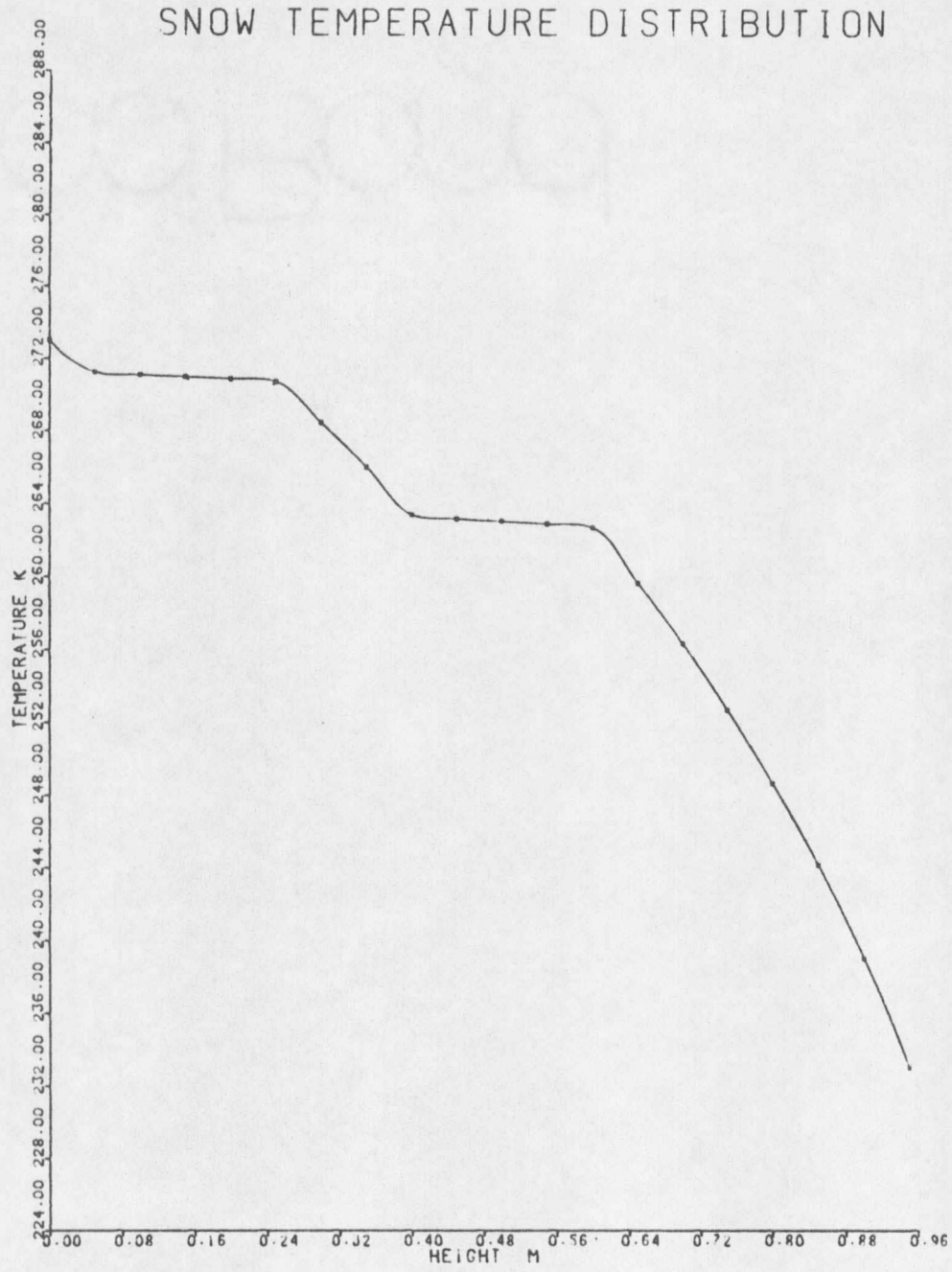

Figure 25. Temperature Profile For Snow Sample 6.

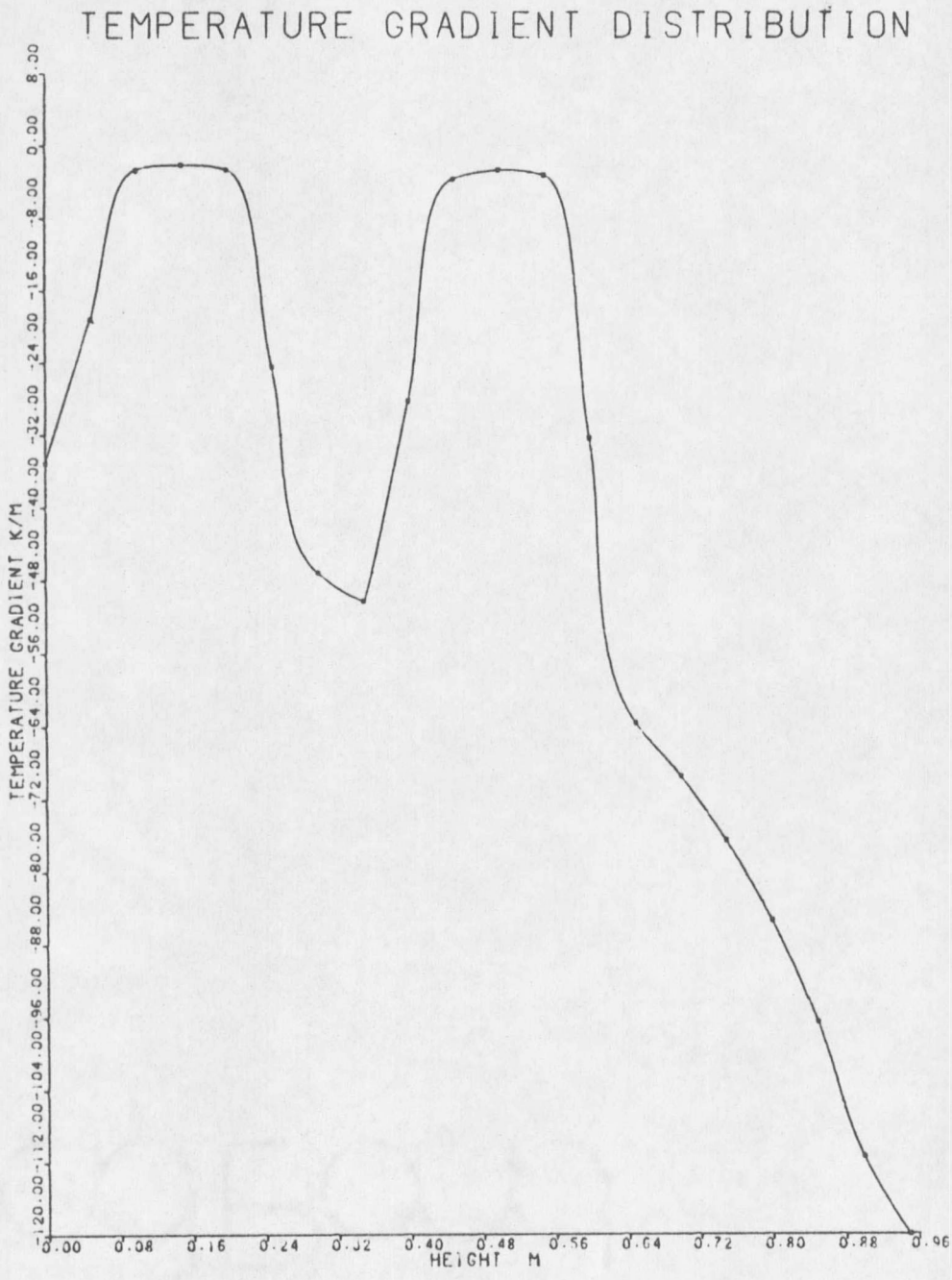

Figure 26. Temperature Gradient Profile For Snow Sample 6.

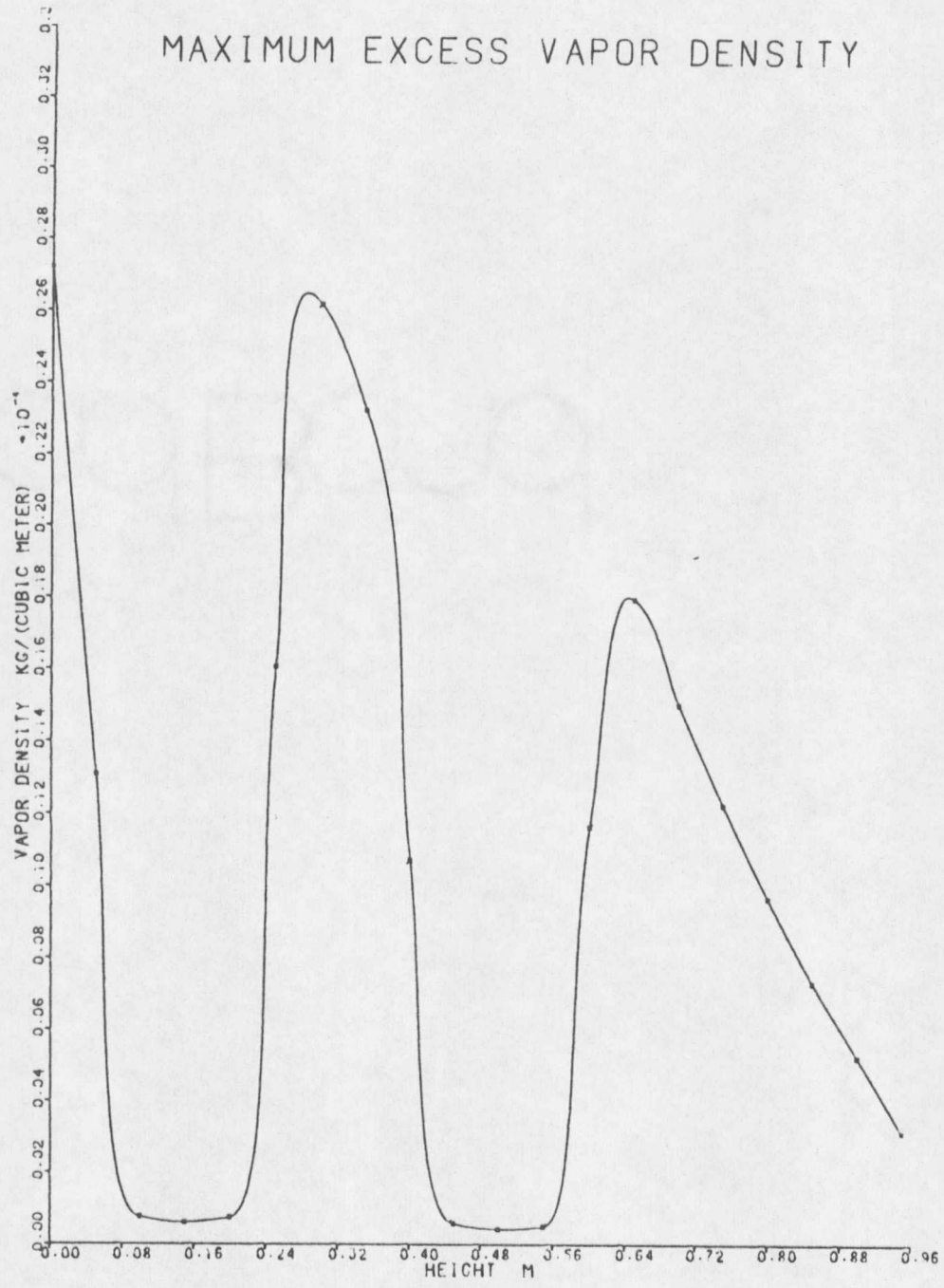

Figure 27. Excess Vapor Density at the Top of the Pore Space Over Flat Surfaced Crystals in Snow Sample 6.

Table 5. Detailed Summary of the Analysis Results for the Pore Space at Each Node, for Snow Sample 6.

Height	Temperature °K	Temperature Gradient Deg m^{-1}	Snow Density $KG \cdot m^{-3}$	Pore Height m.	Pore Pressure PA	Excess Vapor Density $KG \cdot m^{-3} \times 10^{-5}$					
						Bottom of the Pore			Top of the Pore		
						Over Neck	Over Round Surface	Over Flat Surface	Over Neck	Over Round Surface	Over Flat Surface
0.00	273.00	-35.17	100	0.0039	600.49	-2.7231	-2.7159	-2.7141	2.7108	2.7180	2.7198
0.05	271.24	-19.18	100	0.0039	518.94	-1.3113	-1.3050	-1.3034	1.2998	1.3060	1.3076
0.10	271.08	- 2.67	400	0.0016	512.04	-0.7947	-0.7332	-0.7176	0.6781	0.7396	0.7552
0.15	270.97	- 2.14	400	0.0016	507.47	-0.6433	-0.5825	-0.5669	0.5277	0.5886	0.6043
0.20	270.87	- 2.67	400	0.0016	502.94	-0.7687	-0.7082	-0.6928	0.6606	0.7211	0.7365
0.25	270.71	-24.49	100	0.0039	496.27	-1.6086	-1.6026	-1.6011	1.5985	1.6044	1.6059
0.30	268.42	-47.23	100	0.0039	408.90	-2.6175	-2.6125	-2.6113	2.6105	2.6154	2.6166
0.35	265.99	-50.31	100	0.0039	331.58	-2.3228	-2.3187	-2.3176	2.3177	2.3217	2.3227
0.40	263.39	-28.27	100	0.0039	264.03	-1.0722	-1.0689	-1.0681	1.0668	1.0701	1.0709
0.45	263.16	- 3.74	400	0.0016	258.67	-0.0597	-0.0565	-0.0556	0.05396	0.0572	0.0580
0.50	263.01	- 2.78	400	0.0016	255.40	-0.0443	-0.0412	-0.0404	0.0384	0.0415	0.0423
0.55	262.88	- 3.30	400	0.0016	252.37	-0.0518	-0.0487	-0.0479	0.0459	0.0490	0.0498
0.60	262.68	-32.43	100	0.0039	248.01	-1.1642	-1.1611	-1.1603	1.1593	1.1624	1.1631
0.65	259.64	-63.63	100	0.0039	188.45	-1.7941	-1.7917	-1.7911	1.7922	1.7946	1.7951
0.70	256.32	-69.51	100	0.0039	138.74	-1.4993	-1.4975	-1.4971	1.4985	1.5002	1.5006
0.75	252.69	-76.62	100	0.0039	98.26	-1.2216	-1.2203	-1.2200	1.2210	1.2222	1.2225
0.80	248.66	-85.40	100	0.0039	66.27	-0.9634	-0.9625	-0.9623	0.9635	0.9644	0.9646
0.85	244.15	-96.60	100	0.0039	41.96	-0.7288	-0.7282	-0.7281	0.7292	0.7298	0.7299
0.90	239.00	-111.46	100	0.0039	24.40	-0.5211	-0.5208	-0.5207	0.5217	0.5220	0.5221
0.95	233.00	-119.99	100	0.0039	12.58	-0.3121	-0.3120	-0.3119	0.3127	0.3128	0.3129

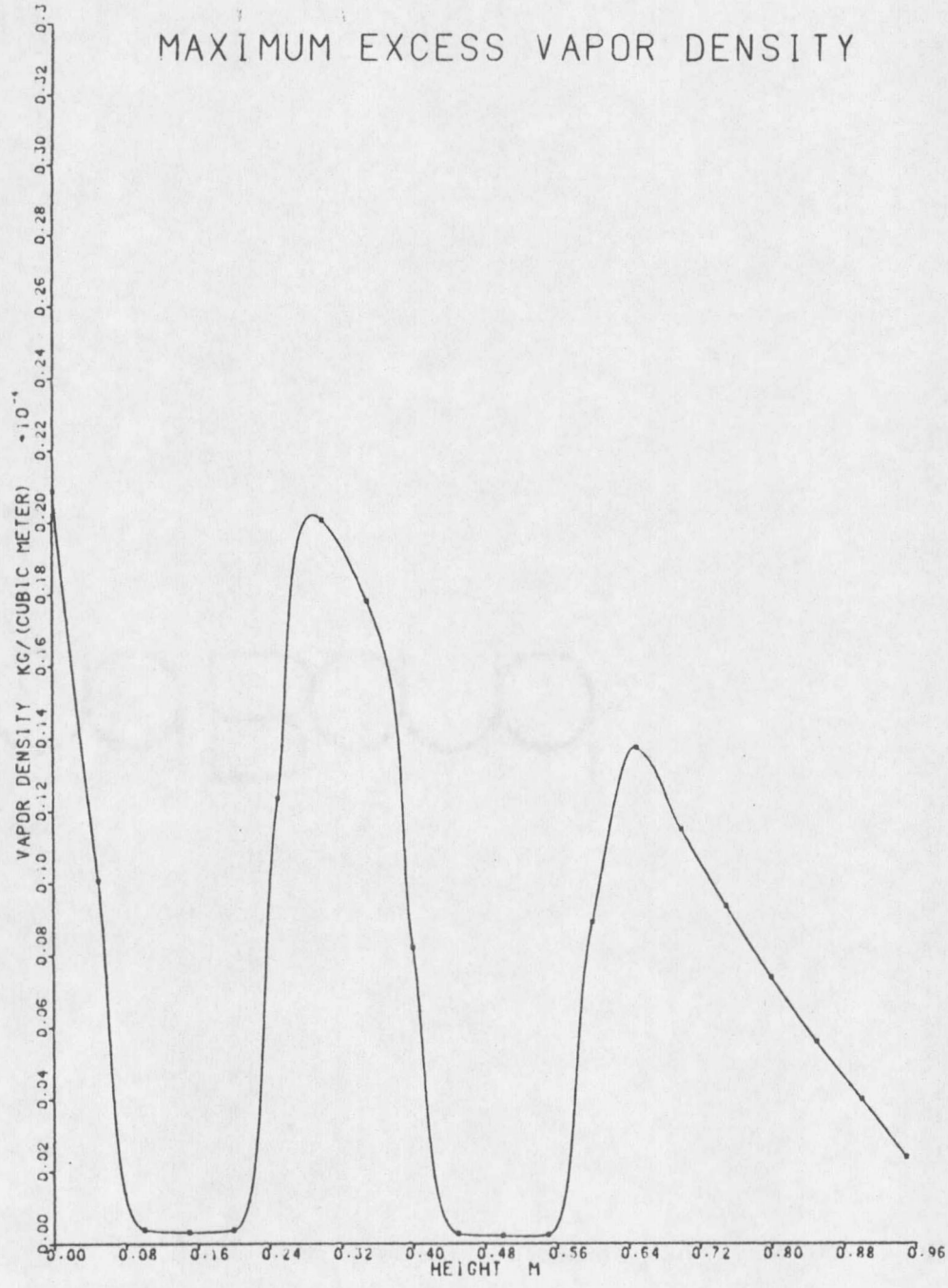

Figure 28. Excess Vapor Density at the Top of the Pore Space Over Flat Surfaced Crystals in Snow Sample 7.

Table 6. Detailed Summary of the Analysis Results for the Pore Space at Each Node, for Snow Sample 7.

Height	Temperature °K	Temperature Gradient Deg m^{-1}	Snow Density $KG \cdot m^{-3}$	Pore Height m	Pore Pressure PA	Excess Vapor Density $KG \cdot m^{-3} \times 10^{-5}$					
						Bottom of the Pore			Top of the Pore		
						Over Neck	Over Round Surface	Over Flat Surface	Over Neck	Over Round Surface	Over Flat Surface
0.00	273.00	-35.16	100	0.0030	600.50	-2.1131	-2.0770	-2.0680	2.0427	2.0785	2.0874
0.05	271.24	-19.18	100	0.0030	518.94	-1.0300	-0.9987	-0.9908	0.9683	0.9995	1.007
0.10	271.08	- 2.67	400	0.0007	512.05	-0.0610	-0.0301	-0.0225	0.0006	0.0315	0.0392
0.15	270.98	- 2.14	400	0.0007	507.48	-0.0546	-0.0240	-0.0164	0.0059	0.0247	0.0323
0.20	270.87	- 2.66	400	0.0007	502.95	-0.0601	-0.0297	-0.0221	0.0006	0.0310	0.0385
0.25	270.71	-24.49	100	0.0030	496.27	-1.2557	-1.2256	-1.2181	1.1973	1.2272	1.2347
0.30	268.42	-47.24	100	0.0030	408.90	-2.0240	-1.9989	-1.9927	1.9757	2.0005	2.0066
0.35	265.99	-50.31	100	0.0030	331.58	-1.7942	-1.7737	-1.7686	1.7553	1.7756	1.7806
0.40	263.39	-28.27	100	0.0030	264.03	-0.8334	-0.8169	-0.8128	0.8020	0.8183	0.8224
0.45	263.16	- 3.74	400	0.0007	258.67	-0.0398	-0.0238	-0.0198	0.0080	0.0241	0.0281
0.50	263.01	- 2.78	400	0.0007	255.40	-0.0031	-0.0172	-0.0133	0.0017	0.0176	0.0215
0.55	262.88	- 3.30	400	0.0007	252.37	-0.0361	-0.0204	-0.0165	0.0051	0.0208	0.0247
0.60	262.68	-32.43	100	0.0030	248.01	-0.9032	-0.8877	-0.8838	0.8733	0.8887	0.8925
0.65	259.64	-63.63	100	0.0030	188.45	-1.3824	-1.3705	-1.3675	1.3605	1.3723	1.3752
0.70	256.32	-69.52	100	0.0030	138.74	-1.1545	-1.1456	-1.1434	1.1384	1.1472	1.1493
0.75	252.69	-76.62	100	0.0030	98.25	-0.9399	-0.9335	-0.9319	0.9282	0.9345	0.9361
0.80	248.66	-85.40	100	0.0030	66.27	-0.7407	-0.7362	-0.7351	0.7331	0.7374	0.7385
0.85	244.15	-96.60	100	0.0030	41.96	-0.5599	-0.5570	-0.5563	0.5552	0.5580	0.5587
0.90	239.00	-111.46	100	0.0030	24.40	-0.4001	-0.3984	-0.3980	0.3975	0.3991	0.3995
0.95	233.00	-119.99	100	0.0030	12.58	-0.2396	-0.2387	-0.2384	0.2383	0.2392	0.2394

Table 7. A Comparison of the Crystal Habits Which Actually Developed in a Laboratory Investigation (Akitaya, 1974) to Those Which are Predicted by the Model.

Temperature at the Center of the Hole °K	Maximum Excess Vapor Density $KG \cdot M^{-3}$	Crystal Habit Predicted by the Model	Crystal Habit Predicted by Akitaya's Diagram	Crystal Habit Which Actually Developed
270.96	0.125×10^{-3}	Plates	Plates	Plates
269.26	0.110×10^{-3}	Needles	Needles	Cups
268.06	0.101×10^{-3}	Needles or Sheaths	Needles or Sheaths	Needles and Sheaths

Chapter VI

SUMMARY

Thermal effects on the metamorphism of dry snow subjected to a temperature gradient are first examined by considering heat flow in a snowpack. Flow of heat, in accordance with basic thermodynamic principles, must be from the ground, which is giving off heat accumulated during the warmer months, toward the snow surface which is at a lower temperature, because it is being cooled by the cold winter air. Heat transfer is considered to take place by thermal conduction, predominately through the solid ice matrix, and diffusion of water vapor across the pore space. Convection is ignored since the extreme conditions necessary to initiate the process are not considered.

An effective thermal conductivity coefficient as a function of temperature and density is developed. This effective conductivity is used instead of the true conductivity because it more adequately represents the transmission of heat, resulting from diffusion as well as pure conduction.

A Fourier heat conduction equation for snow is developed. Application of the equation to a homogeneous snowpack with differing temperature boundary condition yields a non-linear temperature profile. The greater the difference in temperature between the upper and lower boundaries, the greater is the divergence from a linear temperature distribution. Density layering in a snowpack significantly affects the snow temperature distribution and causes a negative spike in the temperature gradient profile above and below high density layers.

To better understand the processes by which faceted crystals develop at the expense of rounded grains, and why a general weakening of the snowpack occurs during tempera-

ture gradient metamorphism, an analysis of the pore space is carried out. Once the temperature distribution in the snow is known, the water vapor pressure within the pore is calculated at nodes placed vertically throughout the pack. This pore vapor pressure is determined by the temperature, temperature gradient, snow density and ice grain geometry. Saturation vapor pressure over the ice surfaces are determined by the mean radius of curvature and temperature. This surface vapor pressure is calculated from the Clausius-Clapeyron and Kelvin equations.

Excess vapor density is defined as the difference between the vapor density in the pore space and that over the ice surfaces. A positive excess vapor density indicates a region of deposition and negative excess vapor density indicates a surface which is losing mass. In the presence of a negative temperature gradient, a negative excess vapor density is established in the lower region of the pore and a positive excess vapor density exists near the top. This indicates a mass flux from the lower toward the upper zones in the pore.

Mass which is deposited at the top of the pore will be in the form of faceted crystals. Negative excess vapor density in the lower region is greatest over the necks, second over the rounded surfaces, and least over the flat surfaces. As a result necks will deteriorate most rapidly, and the percentage of rounded shapes will diminish, since new growth is in the form of faceted crystals.

Crystal habit development in the atmosphere is known to be determined by temperature and excess vapor density. In order to draw a correlation between crystals grown in the atmosphere and those grown in the snowpack, the model presented is examined by considering three experimental cases in a pack, for which the true pore geometry and thermal conditions are known. Actual crystal habits which developed are in agreement

with those which would grow in the atmosphere for the given temperature and the excess vapor density as determined from the model.

A more accurate description of pore size based on the geometric constraints of the snow, such as grain size, crystal type and snow density is needed. This would best be accomplished by a very detailed experimental examination of the pore space for a wide variety of snow types. Other areas which warrant further experimental investigations are the assumptions of a linear temperature profile across the pore and of constant snow density with time.

The theory presented in this paper works well in describing many of the processes which accompany what is generally known as temperature gradient metamorphism, however, a great deal more work needs to be carried out before all of the principles which govern it can be adequately described. The model presented indicates that a reasonable approach to the solution may involve a very detailed and accurate analysis of the processes involved within a single pore space.

REFERENCES

REFERENCES

Adams, E. E., and Brown, R. L. 1982. Further Results on Studies of Temperature Gradient Metamorphism. *J. Glaciology 18(98)*, 205-210.

Akitaya, E. 1974. Studies on Depth Hoar. *Low Temp. Sci. A(26)*, 1-67.

Armstrong, R. L. 1980. An Analysis of Compressive Strain in Adjacent Temperature-Gradient and Equi-Temperature Layers in a Natural Snow Cover. *J. Glaciology 26(94)*, 283-289.

Benson, C. S. 1962. Stratigraphic Studies in Snow and Firn of the Greenland Ice Sheet. *SIPRE Research Report* 70, pp. 1-93.

Bradley, C. C., Brown, R. L., and Williams, T. 1977. On Depth Hoar and the Strength of Snow. *J. Glaciology 18(78)*, 145-147.

Boley, B. A., and Weiner, J. H. 1960. *Theory of Thermal Stresses*. John Wiley and Sons, New York and London.

Colbeck, S. C. 1980. Thermodynamics of Snow Metamorphism Due to Variations in Curvature. *J. Glaciology 26(94)*, 291-301.

Colbeck, S. C. Submitted for publication. The Growth of Faceted Crystals in a Snow Cover.

De Quervain, M. 1963. On the Metamorphism of Snow. In *Ice and Snow*, W. D. Kingery, Editor, MIT Press, Cambridge, Mass., 377-390.

Giddings, J. C., and La Chapelle, E. 1962. The Formation Rate of Depth Hoar. *J. Geophysical Res. 67(6)*, 2377-2382.

Hallet, J., and Mason, B. J. 1958. The Influence of Temperature and Supersaturation on the Habit of Ice Crystals Grown from the Vapor. *Proc. Roy. Soc. Lond. A(247)*, 440-453.

Hobbs, P. V. 1974. *Ice Physics*. Clarendon Press, Oxford.

Kobayashi, T. 1961. The Growth of Snow Crystals at Low Supersaturation. *Phil. Mag. 6* 1363-1370.

Kry, P. R. 1975. Quantitative Stereological Analysis of Grain Bonds in Snow. *J. Glaciology 14(72)*, 467-477.

La Chapelle, E. R. 1969. *Field Guide to Snow Crystals*. University of Washington, Seattle and London.

Marbouty, B. J. 1980. An Experimental Study of Temperature Gradient Metamorphism. *J. Glaciology 26(94)*, 303-312.

Mason, B. J., Bryant, G. W., and Van Den Heuval. 1963. The Growth Habits and Surface Structure of Ice Crystals. *Phil. Mag. 8* 505-526.

Mellor, M. 1964. Properties of Snow. *Cold Regions Science and Engineering Part III Sect AI*. Monograph. U.S. Army Cold Regions Res. and Eng. Lab., Hanover, New Hampshire.

Nakaya, U. 1954. *Snow Crystals*. Harvard Univ. Press, Cambridge, Mass.

Palm, E., and Tusitereid. 1979. On Heat and Mass Flux Through Dry Snow. *J. Geophysical Res. 84(C2)*, 745-749.

Perla, R. I., and Martinelli, Jr., M. 1975. *Avalanche Handbook*. U.S. Dep. Agric., Agric. Handb. 489.

Trabant, D., and Benson, C. 1972. Field Experiment on the Development of Depth Hoar. *Geological Society of America Mem. 135*, 309-322.

Voitkovsky, K. F. et al. 1974. Mass Transfer and Metamorphism in Snow Cover. *Snow Mechanics Symposium IAHS-AISH Publication No. 114*, 16-24.

Yen, Y. C. 1969. Recent Studies in Snow Properties. In *Advances in Hydroscience*, V. T. Chow, Editor, Academic Press, New York, Vol. 5, 173-214.

Yosida, Z. 1963. Physical Properties of Snow. In *Ice and Snow*, W. D. Kingery, Editor1 MIT Press, Cambridge, Mass., 485-527.